JOURNAL OF GEOPHYSICAL RESEARCH, VOL. 113, A09103, doi:10.1029/2008JA013151, 2008

Partially ejected flux ropes: Implications for interplanetary coronal mass ejections

S. E. Gibson[1] and Y. Fan[1]

Received 8 March 2008; revised 9 June 2008; accepted 16 June 2008; published 5 September 2008.

[1] Connecting interplanetary coronal mass ejections (ICMEs) to their solar pre-eruption source requires a clear understanding of how that source may have evolved during eruption. Gibson and Fan (2006a) have presented a three-dimensional numerical magnetohydrodynamic simulation of a CME, which showed how, in the course of eruption, a coronal flux rope may writhe and reconnect both internally and with surrounding fields in a manner that leads to a partial ejection of only part of the rope as a CME. In this paper, we will explicitly describe how the evolution during eruption found in that simulation leads to alterations of the magnetic connectivity, helicity, orientation, and topology of the ejected portion of the rope so that it differs significantly from that of the pre-eruption rope. Moreover, because a significant part of the magnetic helicity remains behind in the lower portion of the rope that survives the eruption, the region is likely to experience further eruptions. These changes would complicate how ICMEs embedded in the solar wind relate to their solar source. In particular, the location and evolution of transient coronal holes, topology of magnetic clouds (''tethered spheromak''), and likelihood of interacting ICMEs would differ significantly from what would be predicted for a CME which did not undergo writhing and partial ejection during eruption.

Citation: Gibson, S. E., and Y. Fan (2008), Partially ejected flux ropes: Implications for interplanetary coronal mass ejections, *J. Geophys. Res.*, *113*, A09103, doi:10.1029/2008JA013151.

1. Background

[2] Solar-driven ''space weather'' can have significantly adverse consequences for the Earth and near-Earth environment. It is therefore important to link geoeffective disturbances in the solar wind to their sources at the Sun, in the hopes of understanding and ultimately predicting their origins. Coronal mass ejections (CMEs) can sometimes be linked causally to solar wind disturbances which possess one or more signatures that identify them as interplanetary coronal mass ejections (ICMEs) [*Gosling*, 1997]. A subset of these exhibit the signature of a rotation of the embedded magnetic field vector: these are referred to as magnetic clouds [*Klein and Burlaga*, 1982]. Observations of both magnetic clouds [*Burlaga et al.*, 1982; *Burlaga*, 1988; *Lepping et al.*, 1990] and CMEs [*Dere et al.*, 1998; *Plunkett et al.*, 2000; *Cremades and Bothmer*, 2004] are commonly interpreted as magnetic flux ropes. Comparisons of flux ropes modeled from interplanetary and coronal signatures have demonstrated agreement of flux rope chirality, axis orientation, and magnetic flux between solar source and magnetic cloud [*Rust et al.*, 2005, and references therein].

[3] The success of such comparisons, however, relies on a clear understanding of how the pre-eruption magnetic configuration in the corona relates to the interplanetary flux rope. There is growing evidence that this relationship is not necessarily straightforward. In particular, evolution during eruption, including rotation and reconnection/interaction with surrounding fields, may need to be taken into account (see *Démoulin* [2008] for a review). In this paper we will examine the interplanetary implications of such evolution using a 3-D numerical CME simulation (originally published by *Gibson and Fan* [2006a]), in which a flux rope writhes and breaks in two during its eruption, with one part escaping as a CME, and the other staying behind in the source region. In section 2 we will briefly review the simulation of *Gibson and Fan* [2006a]. In section 3 we will describe how the surviving portion of the rope may lead to recurring eruptions. In section 4 we will discuss the implications of changes in the connectivity of the escaping rope for transient coronal holes and their association with ICMEs. In section 5 we will discuss how the magnetic helicity, orientation, and even topology of the escaping portion of the rope may be altered during eruption, and how this impacts ICME observations. In section 6 we present our conclusions.

2. A Model for a Partially Ejected Flux Rope

[4] *Gibson and Fan* [2006a] presented a three-dimensional numerical MHD simulation in spherical coordinates, in which a flux rope quasistatically emerged into a preexisting coronal external field. As was the case in previous simulations [*Fan and Gibson*, 2003, 2004; *Fan*, 2005], the emerging rope went through two distinct stages in its

[1]High Altitude Observatory, National Center for Atmospheric Research, Boulder, Colorado, USA.

0148-0227/08/2008JA013151$09.00

evolution. Initially, the rope's quasistatic emergence resulted in a series of equilibria, in which a coronal flux rope was contained within the overlying magnetic fields. Once enough magnetic twist was emerged, however, equilibrium was lost as the magnetic kink instability set in, and the rope erupted.

[5] The simulation described by *Gibson and Fan* [2006a] expanded upon previous analyses by extending long enough in time to demonstrate that the end state of such an eruption was not the total expulsion of the flux rope, but rather a rope that broke in two, with one part leaving, and the other staying behind (see *Gilbert et al.* [2000], *Manchester et al.* [2004a], *Birn et al.* [2006], and *Mackay and van Ballegooijen* [2006] for models of bifurcating flux ropes in coronal eruptions and *Tokman and Bellan* [2002] for an alternative three-dimensional numerical model for splitting filaments). It did so because of a series of reconnections within the rope and between the rope and overlying external fields, which were facilitated by the writhing motion driven by the kink instability. The significance of such a partially ejected flux rope for coronal observations was explored in detail by *Gibson and Fan* [2006b]. We now use the simulation results to explore the implications of a bifurcating magnetic flux rope for ICMEs and space weather.

3. The Rope That Stays Behind: Recurring Eruptions

[6] Figure 1 shows the original flux rope (left) and both the escaping and surviving flux ropes (right). As the rope writhes and expands upward, its legs squeeze together at a central current sheet, leading to reconnections within the rope which split it in two (Figure 2). As we will discuss further in section 4, the escaping portion of the rope continues to reconnect with surrounding external fields as it expands upward, and eventually exits the simulation domain entirely. Meanwhile, the surviving portion of the rope settles down into a new, less-twisted equilibrium state. There is a wide range of observational evidence that such partial ejections of twisted magnetic flux are common, including partly and non-erupting filaments, quiescent filament cavities erupting as 3-part CMEs followed by the reformation of the cavities, and sigmoids transitioning to cusps above reformed sigmoids (Figure 3) [*Gibson and Fan*, 2006b; *Liu et al.*, 2008; D. Tripathi et al., On partially erupting prominences, submitted to *Astronomy and Astrophysics*, 2008].

[7] If a twisted flux rope survives the eruption in this manner, it means that magnetic energy is still stored, and another eruption may soon be triggered. A good example of a repeatedly erupting active region exhibiting signs of partial ejection was described by *Gibson et al.* [2002]. Comprehensive, multiwavelength observations of the region were taken as part of the third Whole Sun Month campaign in August 1999. Multiple flares and at least three CMEs occurred during its disk passage, and these eruptions left cusped soft-X-ray loops behind above ever-present sigmoid (S-shaped) soft-X-ray loops. In particular, Figure 3 shows the cusp in the southern half of the region which resulted from a CME on 14 August, overlying a reformed sigmoid on 16 August. On 17 August there was another CME, leaving behind a cusp over the northern half of the still sigmoid region, as well as a filament which did not participate in the eruption. On 20 August there was a flare with cusped post-flared loops, an extreme-ultraviolet dimming, and a portion of the filament disappeared, all in the southern half of the region. On 21 August, however, the sigmoid was back, more clear than ever. Finally, as the region rounded the west limb, a CME occurred in its vicinity, including an especially well-observed jet [*Ko et al.*, 2005].

[8] The cusps over reformed sigmoids and non-erupting or partially erupting filaments observed in this region are consistent with modeling it as a magnetic flux rope which repeatedly expels part, but not all, of its twisted magnetic fields in CMEs. In this scenario, each eruption leaves enough twist behind for a sigmoid separatrix surface to survive, which continues to be observable as a quiescent soft-X-ray sigmoid [*Fan and Gibson*, 2006]. New flux emerges (as was observed and discussed by *Gibson et al.* [2002]), leading to further losses of the rope's equilibrium, perhaps due to threshold limits on magnetic twist or helicity [*Fan and Gibson*, 2007]. Such repeated partial ejections from a single region may have space weather significance, if for example their interaction leads to particularly strong solar energetic particle (SEP) events [*Gopalswamy et al.*, 2004].

4. Jumping Ropes: Changes in Magnetic Connectivity

4.1. Transient Coronal Holes: Location and Morphology

[9] Transient coronal holes (TCHs) are associated with CMEs, and appear as dimmings in soft X-ray [*Sterling and Hudson*, 1997; *Hudson et al.*, 1998] and extreme ultraviolet [*Thompson et al.*, 1998, 2000] (Figure 6c) and brightenings in the infrared HeI line [*de Toma et al.*, 2005]. They have been proposed to be the foot points of magnetic clouds [*Webb et al.*, 2000]. In some cases, double-dimmings lying in the concavity of a sigmoid neutral line have been observed [*Sterling and Hudson*, 1997], in a manner demonstrated by *Gibson and Low* [2000] to be consistent with the modeled expansion of a flux rope. That study made use of an expanding flux rope which existed prior to eruption, but the basic conclusions regarding the location and morphology of dimmings are equally consistent with an expanding flux rope formed in situ in the early stage of the eruption [e.g., *Moore and Labonte*, 1980; *Gosling*, 1990; *Qiu et al.*, 2007].

[10] However, *Kahler and Hudson* [2001] found cases where the TCHs do not lie in strong field source regions within curved neutral line, but rather extend out into nearby weaker field regions. In such cases, the TCHs may occupy significantly larger area than the associated flaring active region [*Thompson et al.*, 2000; *Zhukov and Veselovsky*, 2007; *Attrill et al.*, 2007]. These observations strongly indicate that reconnections between erupting structures and surrounding fields have resulted in escaping fields rooted external to the source.

[11] Figure 4 demonstrates how this might occur. As the escaping portion of our rope expands upward, its outer edge writhes counterclockwise beneath the overlying external fields, driving reconnections between the escaping rope

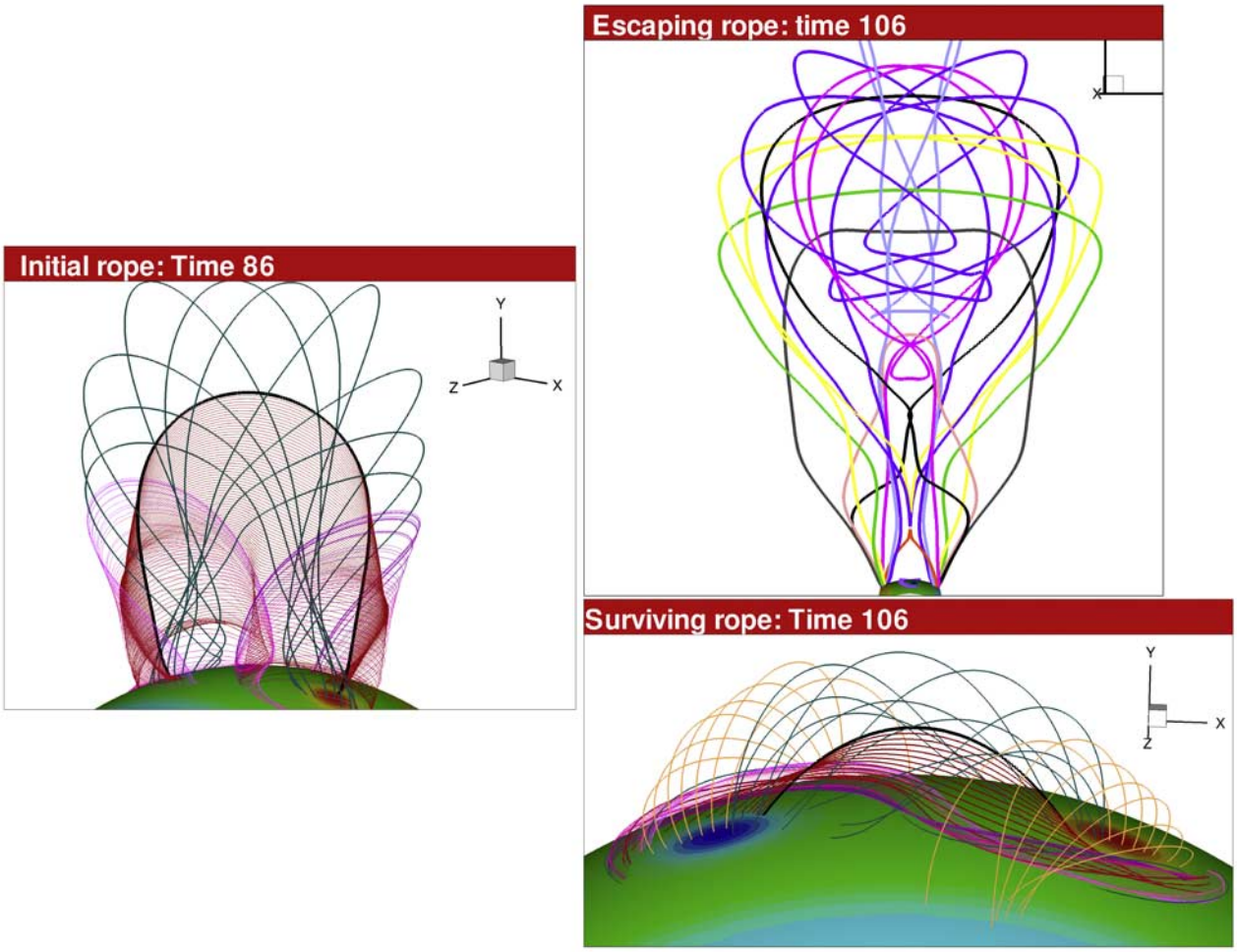

Figure 1. Bifurcating flux rope. The left image shows sample field lines for the pre-eruption flux rope. Red and black field lines are dipped field lines intersecting the central *y* axis, pink-lavender are winding field lines grazing the photosphere, and dark green and blue are additional rope field lines. The two right images show the bifurcated rope later in its eruption. The top right image shows sample field lines of the escaping rope, which are rooted in the external boundary. The bottom right image shows sample field lines of the surviving rope, color-coded in the manner of the original rope. The surviving rope is rooted in the rope bipole, but some adjacent field lines (e.g., the orange ones in this image) have one foot point in the rope-bipole boundary and one in the external boundary. The lower boundary on all images shows color contours of radial magnetic field (red positive, blue negative).

and the external fields and forming ''mixed-connectivity'' field lines (that is, one foot point in the original external field boundary, the other in the original rope-bipole boundary). These mixed-connectivity escaping field lines subsequently reconnect at a central current sheet, and in the process remove the final attachments between the escaping field and the original rope-bipole boundary (Figure 5). The result is an escaping rope rooted in the lower boundary of what was originally (pre-eruption) external fields unconnected to the emerging flux rope. This can be seen in Figure 1 (top right) which shows the escaping rope's field lines lie outside the original rope bipolar magnetic region. Thus the feet of the CME escaping flux rope have lost their connection to the original source [*Gibson and Fan*, 2006b, 2006c] [see also *Roussev et al.*, 2007]. If we identify the dimmings with the feet of the escaping flux rope, they would lie external to the strong magnetic bipole, in the weaker surrounding fields (Figure 6), as often observed.

[12] Both the initial, emerging flux rope and the overlying initial external fields in our simulation are very symmetric. For this reason, the reconnections between the two magnetic systems lead to a symmetric escaping rope with twin, symmetric dimmings at its feet. The right-hand image of Figure 6c shows a case where, although the dimmings are twin and highly symmetric, they extend well above and below the flaring active region in weaker field, and are not concentrated in the concavities of the associated sigmoid [*Thompson et al.*, 2000]. As Figure 6b shows, the escaping rope feet of our simulation match this configuration well. Note, however, that *Attrill et al.* [2006] analyzed this event in detail, and concluded that the asymmetric temporal and spatial evolution of the region actually implied that only the southernmost dimming was a foot points of the magnetic

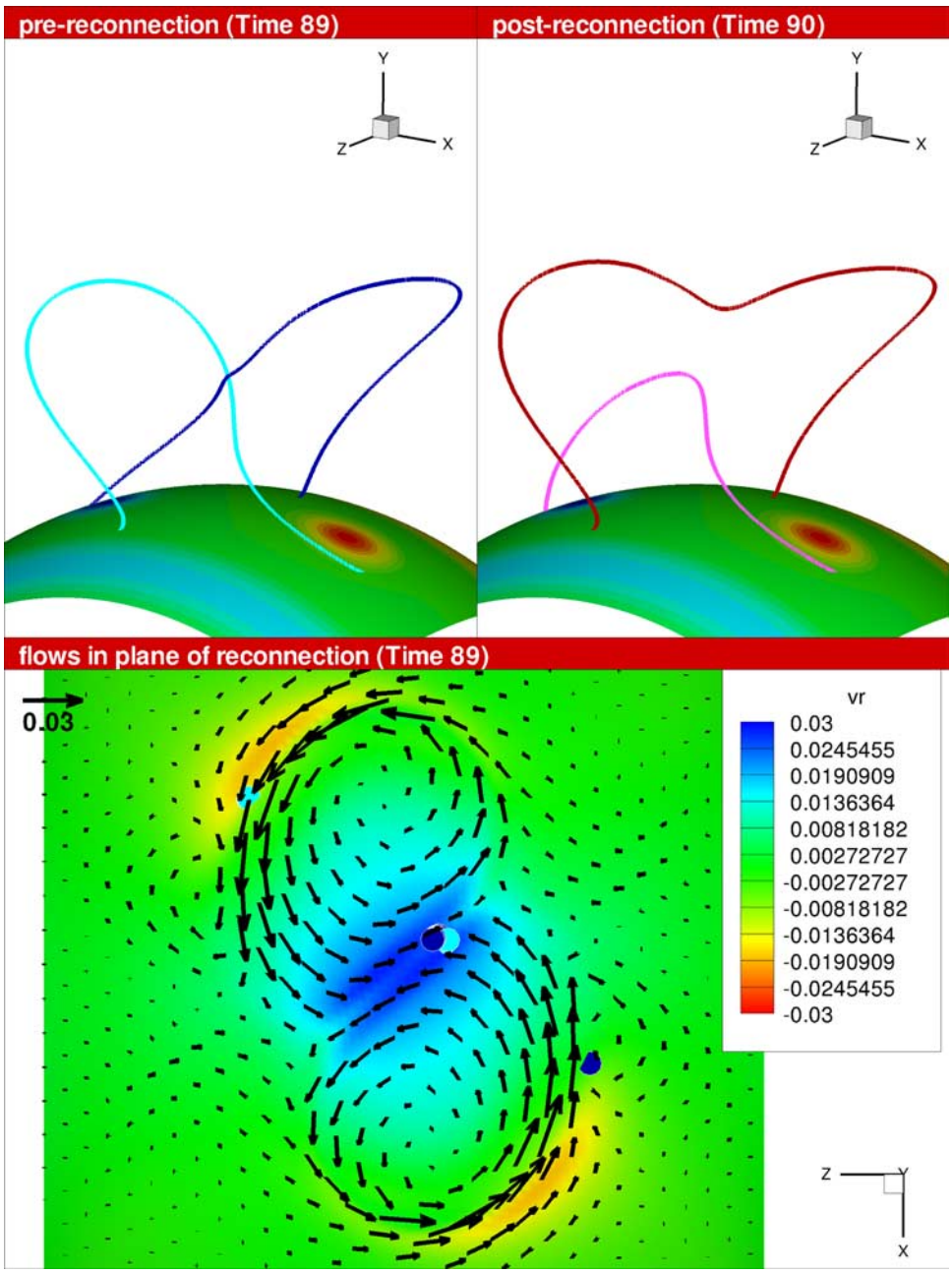

Figure 2. Rope-breaking reconnection. Left-hand top image shows two field lines (blue) just prior to reconnection. Right-hand top image shows two field lines (red/pink) at the next time step which originate from the same points on the lower boundary as the blue field lines of the previous time step. These have clearly undergone reconnection, resulting in one (red) expanding upward and one (pink) falling back down. The lower boundary on the top images shows color contours of radial magnetic field (red positive, blue negative). The bottom image shows a velocity contour slice at the height of the reconnection point at the pre-reconnection time, which is intersected by the two blue field lines at the points shown. This demonstrates the converging motion of the field lines at the reconnection point. (See dynamic content Animation 1 in the HTML for a movie of the magnetic field lines rotating in three dimensions.[1])

cloud, while the northern portion of the erupting structure had reconnected with the open field of the northern coronal hole, thus detaching it. This interchange reconnection between erupting and polar hole fields was also concluded on the basis of interplanetary observations of the corresponding magnetic cloud [*Crooker and Webb*, 2006]. In general, the evolution of TCHs is likely to be very sensitive to the form of surrounding large-scale fields, and it is clear that asymmetric, solo, or patchy and widespread dimmings might occur during a partial ejection depending upon this form

[1]Animations are available in the HTML.

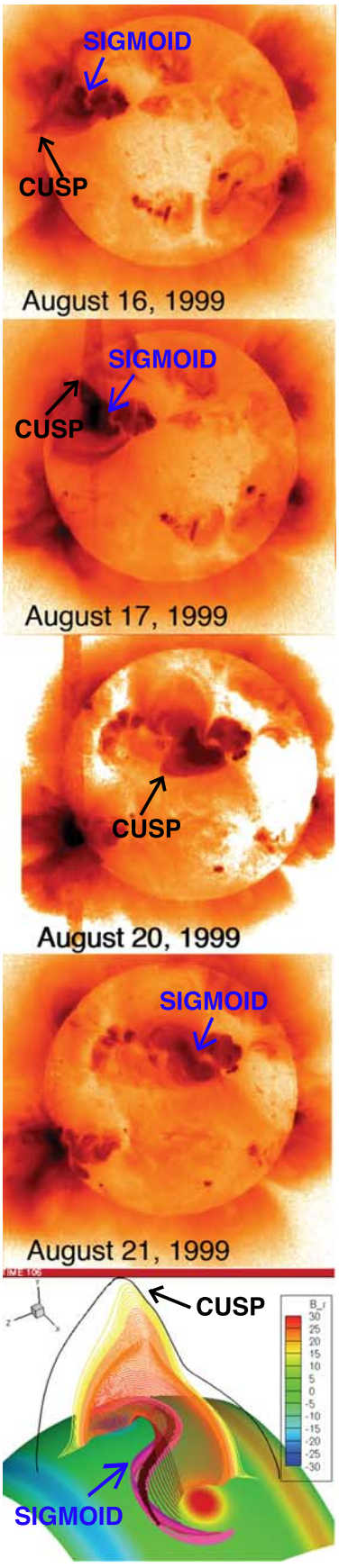

[see, e.g., *Delannee*, 2000; *Delannee et al.*, 2007; *Mandrini et al.*, 2005, 2007; *Attrill et al.*, 2007; *Zhang et al.*, 2007; *Zhukov and Veselovsky*, 2007].

4.2. Transient Coronal Holes: Evolution

[13] As the escaping rope continues to expand upward, further reconnections eventually occur as the radially pulled field lines meet at the central current sheet behind the rope, ultimately severing the escaping rope's connection to the Sun (Figure 7). In the two (or two and a half) dimensional standard model of an eruptive flare [e.g., *Hirayama*, 1974] these "close-down" reconnections are essentially identical to the "flux-detaching" reconnections which may begin quite early in the eruption, adding twist to the core of the erupting structure and leaving behind a post-eruptive arcade and two-ribbon flare. However, in our three-dimensional model, the flux-detaching reconnections of Figure 5 and the close-down reconnections of Figure 7 are distinct. The flux-detaching reconnections occur as described above between mixed-connectivity field lines relatively early in the eruption, severing the connection to the original rope-bipole and leaving behind post-eruptive arcade and flare ribbons [*Gibson and Fan*, 2006b]. In the process they also add significant helicity to the escaping portion of the rope as we will discuss below, and so play an "in situ" role in forming the escaping rope. The reconnection shown at simulation time step 106 in Figure 5 is one of the last of this type. After this time the close-down reconnections continue, but differ from the earlier flux-detaching reconnections in that they occur between field lines rooted entirely external to the original rope-bipole boundary. It is important to point out that in these close-down reconnections we do not generally see an individual field line's "legs" coming together and self-connecting, which is a two-dimensional picture and unlikely to occur in three dimensions [*Gosling et al.*, 1995]. Rather, neighboring field lines reconnect with each other multiple times, resulting in some highly twisted core field lines in the escaping rope (we will return to this point in section 5.3.3), and an outwardly progressing close-down of the coronal field.

[14] Figure 8 demonstrates the model prediction for TCH evolution. In Figure 8 we have plotted two types of field line foot points. The black ones are, as in Figure 6, the foot points of escaping rope field lines that have reached the upper boundary of the simulation. The colored dots are foot points of field lines that are twice as long as the field lines originating from these points at time step 86 (when flux rope emergence was stopped in the simulation). (Note that we also compare to the field lines originating from these points at the immediately preceding time step (thus a "running difference") and eliminate the foot points of any field line which is shrinking or has just undergone recon-

Figure 3. Yohkoh SXT observations of an active region which erupted multiple times between 15 and 21 August 1999 (image is in negative color table; dark indicates strong soft-X-ray (SXR) emission). Cusped field lines resulting from eruptions apparently overlie sigmoid-shaped loops throughout the active regions disk passage, in the manner predicted by the partially ejected flux rope model (bottom panel; image from *Gibson and Fan* [2006b]).

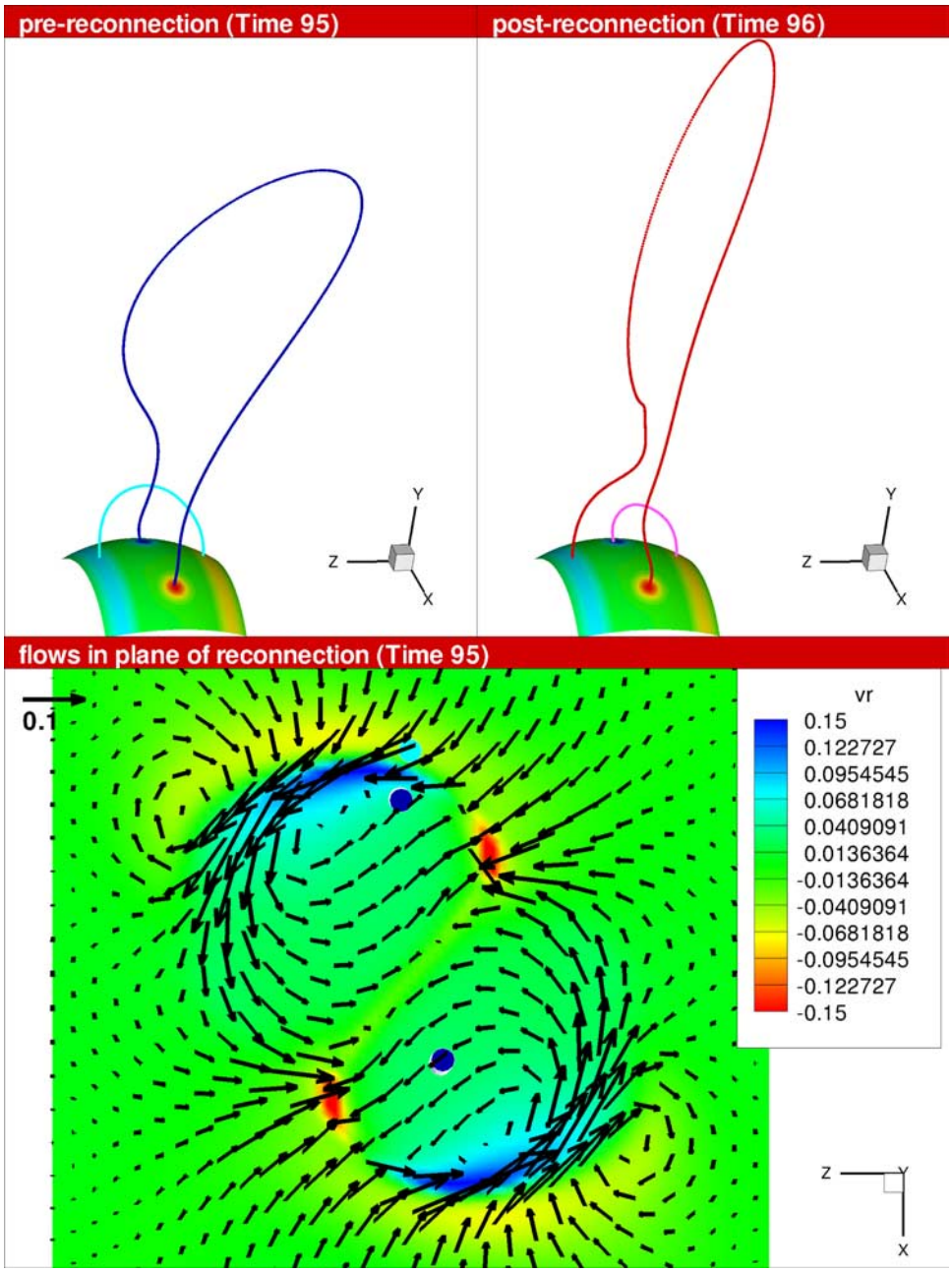

Figure 4. Arcade-rope connectivity-mixing reconnection. As in Figure 2, top images show pre-reconnection and post-reconnection field lines, and bottom image illustrates the convergence of the pre-reconnection field lines. (See dynamic content Animation 2 in the HTML for a movie of the magnetic field lines rotating in three dimensions.)

nection.) The colors indicate the connectivity of field lines (see Figure 8 caption). It has been argued that TCHs may correspond to the foot points of all field lines initially stretched upward by the erupting core, whether or not they are ultimately the foot points of the escaping rope [*Mandrini et al.*, 2005, 2007]. We see from Figure 8 (left column) that the foot points of such stretched-out field lines appear first within the rope-bipole boundary (purple points), and then extend outward into surrounding fields until flux-detaching reconnections separate the escaping rope from the initial rope-bipole boundary as described above (transition of purple points to dark green and then red), leaving behind the true "feet" of the escaping rope field lines (transition of red points to black). Figure 8 (right column) then demonstrates how these black points are eventually removed as the escaping rope is gradually detached via close-down reconnections.

[15] The model prediction for TCH boundary evolution illustrated by Figure 8 is consistent with observations of TCH boundaries migrating outward from the core active region [e.g., *Kahler and Hudson*, 2001]. In particular, the model is consistent with TCHs which originate within the

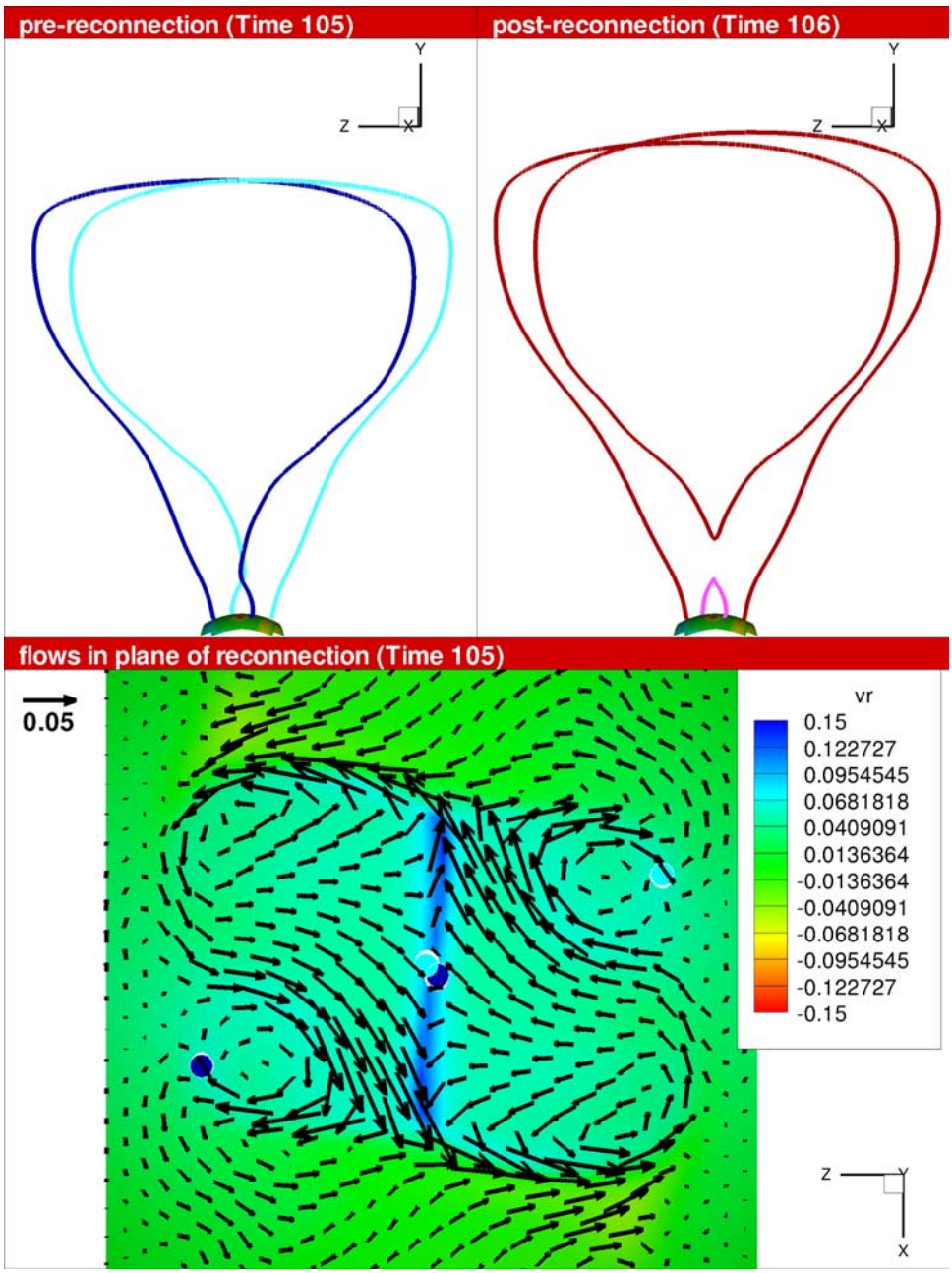

Figure 5. Flux-detaching reconnection. As in Figure 2, top images show pre-reconnection and post-reconnection field lines, and bottom image illustrates the convergence of the pre-reconnection field lines. Note that both of the blue pre-reconnection field lines are "mixed" connectivity, with one foot point in the original external field boundary and the other in the original rope-bipole boundary, but that the post-reconnection the escaping flux rope field line has both feet in the external field boundary. (See dynamic content Animation 3 in the HTML for a movie of the magnetic field lines rotating in three dimensions.)

core of an active region, reach a maximum extent covering both the core and some external weaker field regions, start to fill in at the central "core" as post-eruptive arcades form, and then survive for some time as TCHs external to the original core region until they disappear as close-down reconnections sever the escaping rope's link to the Sun. *McIntosh et al.* [2007] showed multiple observed examples where TCHs initially dimmed in the opposing poles of the active region (i.e., core dimmings), subsequently extended outward, and then filled in beginning with the core dimmings. It is also consistent with the observations of *Reinard and Biesecker* [2008], who showed that a large minority (30%) of TCHs studied (96 total), exhibited a "two-slope" recovery of intensity. Thus, the initial filling-in of TCHs occurs quickly (Figure 8 (left column)), in roughly the same amount of time as it takes for them to reach their maximum

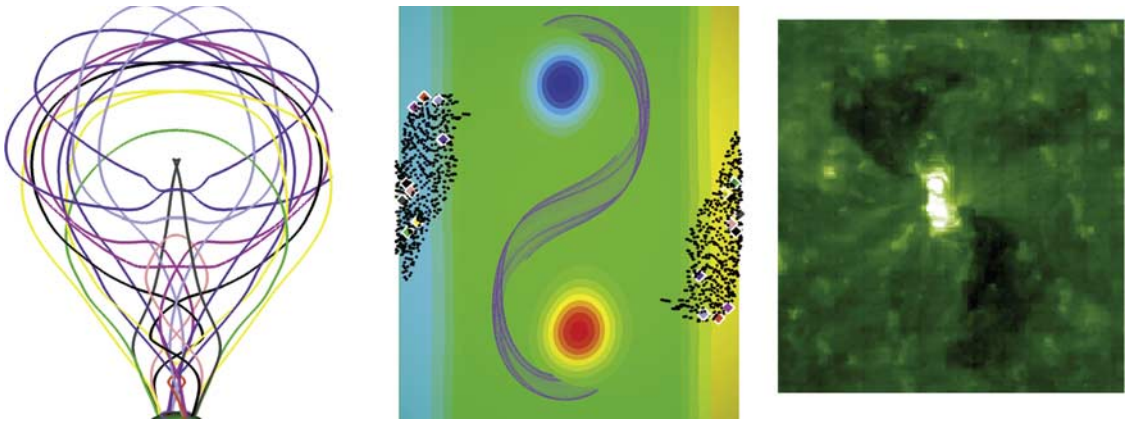

Figure 6. (left) Colored field lines show sample field lines of escaping flux rope at simulation time step 106. (middle) Purple field lines show surviving rope; colored diamonds correspond to foot points of escaping rope field lines from image to left; black dots show more foot points of escaping rope field lines obtained by tracing all field lines exiting the top of the simulation box ($10R_{\odot}$) down to the lower boundary. Colored isocontours show radial magnetic flux, indicating that the escaping flux rope foot points lie outside the original rope bipole. (right) SOHO/EIT 195 Angstrom observations of transient coronal holes of 12 May 1997 [*Thompson et al.*, 1998].

net depletion, and then a second, more gradual filling-in of the TCHs continues lasting several hours (Figure 8 (right column)). We have confirmed that in some cases (e.g., 23 July 1999) it can be established that the initial steep slope corresponds to an early and quick filling-in of the core dimmings, and the flatter, secondary slope corresponds to a slower filling-in of dimmings outside the original active region, in a manner consistent with our model (A. Reinard, private communication, 2008).

[16] Finally, it is worth noting that even at the end of the simulation run (time step 173) when all significant helicity of the escaping rope has expanded out of the system (see section 5.1), not all the flux of the escaping rope has closed down. This is consistent with observations of magnetic clouds that imply that at least some of the flux rope is still attached to the Sun when it passes 1 AU. It is also consistent with observations of TCHs which show them lasting for many hours [*Kahler and Hudson*, 2001].

4.3. Implications for Magnetic Cloud Flux

[17] We refer to the reconnection shown in Figure 5 as flux-detaching, and Figure 5 demonstrates how the final attachments to the original rope-bipole boundary are severed. Decreasing the connection to the photosphere may be seen as equivalent to increasing the azimuthal flux, or winding, in the escaping rope. It is a subject of current controversy as to how the magnetic flux associated with dimmings maps to that within magnetic clouds [*Démoulin*, 2008]. In particular, some authors find that the magnetic flux in TCHs map well to the axial flux in a magnetic cloud [*Qiu et al.*, 2007], as might be expected if TCHs correspond to the foot points of an expanding magnetic flux rope, either preexisting or formed in situ early in the eruption. Other authors [*Mandrini et al.*, 2005, 2007] have shown cases where only a fraction of the TCH-associated flux maps to the axial flux of the magnetic cloud, as would be consistent if much of the TCH corresponds to the foot points of stretched-out field lines which are not ultimately connected to the escaping rope (as discussed above). In this scenario these expanding fields would reconnect with the core sheared field late in its eruption (e.g., as described by *Lin and Forbes* [2000]), adding to the escaping rope's azimuthal, rather than axial flux.

[18] Our model differs from both of these scenarios. Flux-detaching reconnections set in only after a significant amount of stretching has occurred on many field lines, as in the case of the scenario described by *Mandrini et al.* [2005, 2007]. However, unlike that scenario, in which flux-detaching reconnections serve to break the connection of the escaping rope to external fields, the flux-detaching reconnections in our model remove the connections to the original core flux. This difference arises because of the rotation that the rope undergoes during our model eruption: indeed, observations of the evolution of TCH boundaries may be a means of determining whether an eruption involves such a rotation. As we will show below, the result of such a rotation may be topological changes which blur the distinctions between axial and azimuthal field.

5. Forming Tori: Changes in Magnetic Helicity, Orientation, and Topology

5.1. Changes in Magnetic Helicity

[19] Magnetic helicity is a global property measuring the amount of twist or shear in a magnetic field relative to its potential state. On time-scales which are very large compared to that of CMEs and flares, global magnetic helicity is conserved [*Berger and Field*, 1984]. The CME represents a mechanism by which magnetic helicity may be carried away from the Sun. For this reason, efforts have been made to compare magnetic helicity in magnetic clouds to magnetic helicity of their "source" regions (see *Démoulin* [2008] for a review). Such studies have made it clear that reconnections during eruption may significantly impact the helicity in the magnetic cloud, as mutual helicity between the source

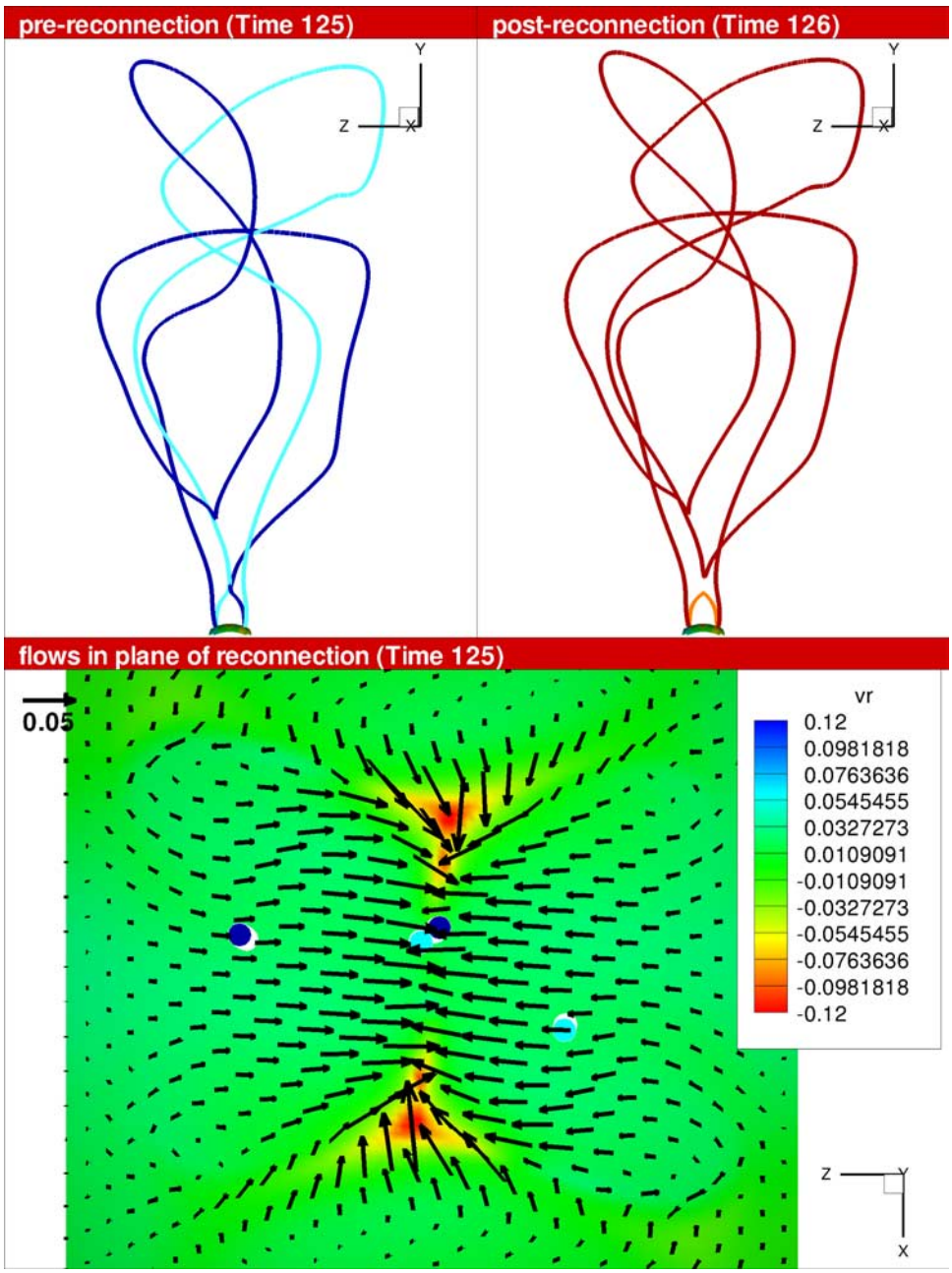

Figure 7. Flux-close-down reconnection. As in Figure 2, top images show pre-reconnection and post-reconnection field lines, and bottom image illustrates the convergence of the pre-reconnection field lines. Note that both of the blue pre-reconnection field lines have both feet in the original external field boundary. (See dynamic content Animation 4 in the HTML for a movie of the magnetic field lines rotating in three dimensions.)

region and its surroundings is transformed into self-helicity of an escaping flux rope [*Leamon et al.*, 2004].

[20] Our simulation is initiated by the destabilization of a preexisting magnetic flux rope. However, the reconnections during its eruption greatly affect what ultimately escapes to become a magnetic cloud. We have already discussed connectivity changes due to these reconnections, and we now demonstrate that they also serve to add helicity from surrounding fields (i.e., mutual helicity) to the escaping portion of the rope.

5.1.1. Quantifying Magnetic Helicity Transfer

[21] Figure 4 illustrates how mutual helicity between the original rope and surrounding field are introduced to the escaping rope. The light blue field line is a simple, unsheared arcade-like field line. The dark blue field line is part of the original flux rope, and as such has a noticeable amount of shear. It is also oriented essentially at a right angle to the light blue field line. When they reconnect, they form the escaping, dark red field line which now has all of the shear of the original dark blue flux rope line, but also an

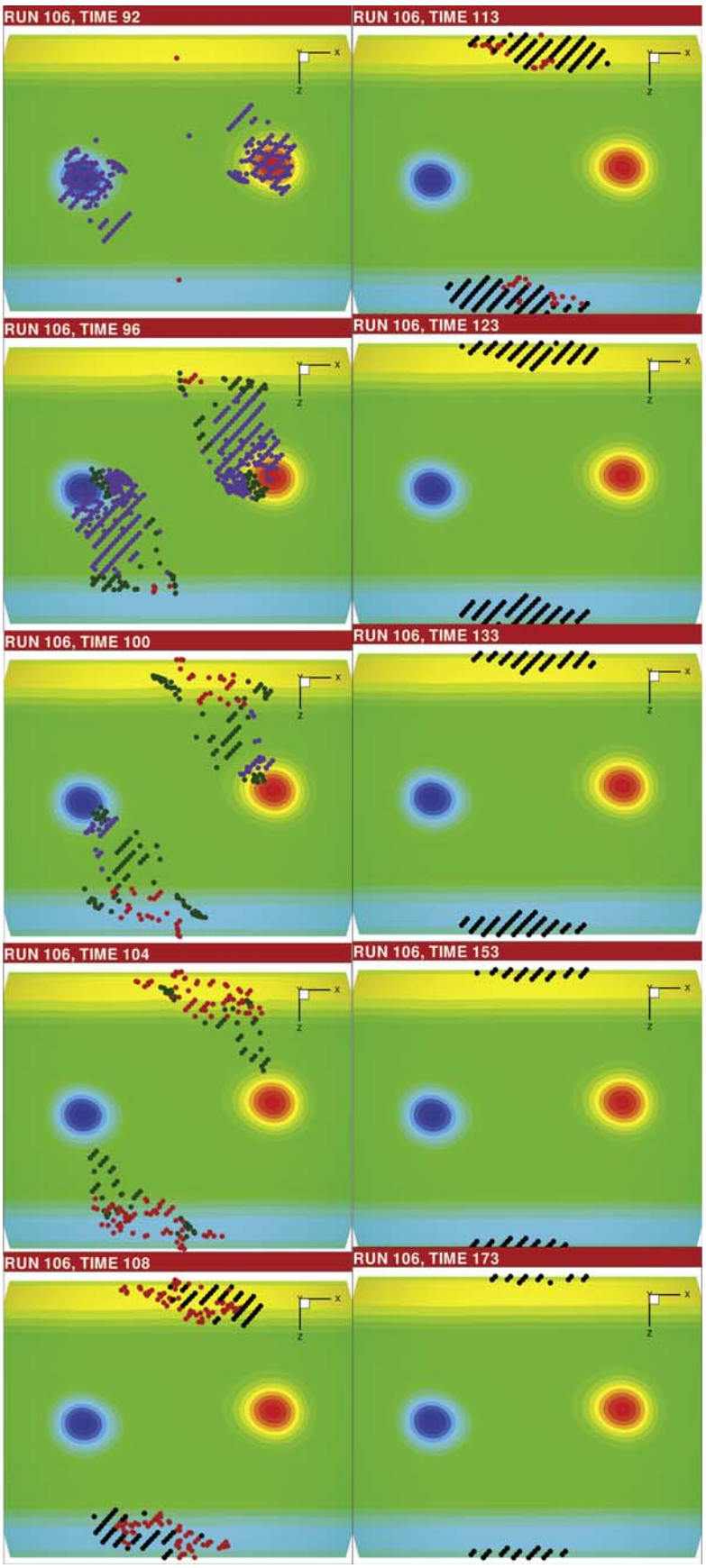
RUN 106, TIME 92
RUN 106, TIME 113
RUN 106, TIME 96
RUN 106, TIME 123
RUN 106, TIME 100
RUN 106, TIME 133
RUN 106, TIME 104
RUN 106, TIME 153
RUN 106, TIME 108
RUN 106, TIME 173

Figure 8

additional kink where the field lines have reconnected at right angles. When these mixed-connectivity type field lines reconnect at the central current sheet, they form the escaping flux rope field lines, e.g., the dark red field line of Figure 5, which clearly have more twist than the dark blue original flux rope field line of Figure 4.

[22] We can quantify this transfer of mutual helicity to the escaping rope. We can calculate the total magnetic helicity in our simulation box, before the rope loses equilibrium and erupts, $H_{pre_{total}}$ [*Fan and Gibson*, 2007]. Because the magnetic flux rope being emerged is defined analytically [*Fan*, 2005], we can also define that pre-eruption rope's self-helicity, $H_{pre_{self}}$. Given these two values, because the pre-reconnection external field is potential and so has no self-helicity, we are able to explicitly calculate the mutual helicity between the rope and surrounding fields, $H_{pre_{mutual}}$. Thus,

$$H_{pre_{mutual}} = H_{pre_{total}} - H_{pre_{self}} \quad (1)$$

[23] We find that in the original configuration, 38% of the helicity was in the form of the flux rope's self-helicity, and 62% in the form of mutual helicity.

[24] Once the escaping portion of the rope has left the simulation box, we can calculate the total helicity left in the box, $H_{post_{total}}$. We are thus able to quantify the amount of helicity leaving with the escaping rope, i.e.,

$$H_{post_{escape}} = H_{pre_{total}} - H_{post_{total}} \quad (2)$$

[25] We find in this manner that 41% of the helicity in the original system is lost with the escaping rope, while 59% remains. Owing to the transfer of mutual helicity to the escaping rope, it leaves with (slightly) more helicity than the pre-eruption rope had, yet still leaves behind a surviving twisted magnetic flux rope (Figure 1).

5.1.2. Implications for Magnetic Cloud Twist

[26] Magnetic helicity is related to magnetic twist, or winding number, via magnetic flux. Thus, a standard magnetic flux rope possessing field lines which are all anchored at a lower boundary will have an average winding number equal to the magnetic helicity of the volume divided by square of the magnetic flux through the rope's lower boundary. If field lines are detached from this lower boundary, the amount of flux through the lower boundary decreases and the winding number increases. This is evident in Figure 1, where, despite the fact the original and escaping ropes have approximately the same amount of helicity, the escaping rope winds much more. Thus, Figure 4 demonstrates how mutual helicity is added to the escaping rope, and Figures 5 and 7 show how the winding number increases as field lines are detached from the photosphere. In a simple, cylindrical flux rope, this increase in winding number is equivalent to adding azimuthal flux to the rope. *Qiu and Yurchyshyn* [2005] have demonstrated that the azimuthal flux in magnetic clouds is equivalent in magnitude to the "reconnection flux" swept up by separating flare ribbons, as would be expected if the ribbons show the foot points of field lines undergoing flux-detaching reconnections. This is essentially consistent with our simulation results, since the majority of the twist in our escaping rope arises from such flux-detaching reconnections. However, as we will demonstrate below, separating the axial and azimuthal flux in our escaping rope is not straightforward.

5.2. Changes in Rope Orientation

5.2.1. Writhing Filaments

[27] In section 2 we described how the magnetic kink instability led to the loss of equilibrium of the emerging flux rope. As the rope erupted, it writhed in a manner that facilitated its rupture through overlying fields [*Fan*, 2005] (Figure 9b). Observations of writhing motions such as shown in Figure 9a have been reported in filament eruptions of all sorts (e.g., full, partial, or failed) [*Ji et al.*, 2003; *Rust and Labonte*, 2005; *Williams et al.*, 2005; *Alexander et al.*, 2006; *Zhou et al.*, 2006; *Liu et al.*, 2007, 2008; *Gilbert et al.*, 2007]. Writhing motions have also been observed in the cores of white light CMEs, which are identified with erupting filaments (Figure 10 (top row)). *Gibson and Fan* [2006b] simulated the filament eruption by tracking the plasma of material initially lying within the dips of the magnetic field. Figure 10 (middle and bottom rows) shows that such entrained mass exhibits writhe similar to that seen in erupting filaments and the white light core of the CME, of approximately 115 degrees counterclockwise relative to its original orientation. Because our rope is left-handed (negative helicity), this is consistent with the observational study of *Green et al.* [2007], who analyzed several cases of filament writhe and found that counterclockwise (clockwise) writhe was associated with negative (positive) helicity.

5.2.2. Implications for Magnetic Cloud Rotation

[28] Magnetic clouds are characterized by a rotation of the magnetic field vector [*Klein and Burlaga*, 1982]. Comparisons between the orientation of the magnetic cloud field and magnetic structures back at the Sun have revealed correlations. For example the leading polarity of magnetic clouds appears to vary with the solar cycle to reflect the direction of the global solar dipole [*Bothmer and Schwenn*,

Figure 8. Time series of field line foot points representing (left column) early evolution of transient coronal holes, as flux-detaching reconnections transfer the connectivity of expanding field lines from the original rope-bipole boundary to the external-field boundary, and (right column) the continuing evolution of transient coronal holes as close-down reconnections remove the connection of the escaping rope to the lower boundary. Note that the time spacing differs between the two columns. Colored dots are the foot points of field lines that have expanded to twice their initial length: purple are if both feet are rooted in the original rope-bipole boundary, red indicate both feet rooted in the original external-field boundary, and dark green indicate "mixed connectivity", with one foot in each boundary. Black dots are foot points of field lines which have reached the top of the simulation box. The colored isocontours indicate radial magnetic field at the simulation lower boundary (red positive, blue negative). (See dynamic content Animation 5 in the HTML for a movie animating this time evolution.)

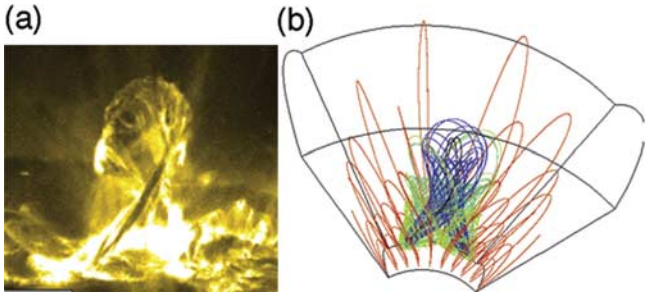

Figure 9. (a) TRACE 195 Angstrom image of writhing filament 27 May 2002 (see *Ji et al.* [2003], *Rust* [2003], *Alexander et al.* [2006], and *Toeroek and Kliem* [2005] for analyses of this region). (b) Writhing flux rope (blue and green field lines) before most of the reconnections with external (red field lines) have occurred (simulation time step 86). Note we have flipped the TRACE filament horizontally so as to compare to the model flux rope (which writhes counterclockwise).

1997; *Mulligan et al.*, 1998] (although the timing of magnetic cloud polarity change versus that of the solar dipole are not simultaneous [*Li and Luhmann*, 2004]). Moreover, numerous cases have been demonstrated where the orientation of the magnetic cloud axis is aligned with that of a solar filament prior to its eruption [*Bothmer and Schwenn*, 1997; *Marubashi*, 1997; *Yurchyshyn et al.*, 2001; *Rust et al.*, 2005; *Yurchyshyn et al.*, 2006]. For such cases where a filament eruption is linked temporally and spatially to a magnetic cloud, there is a subset which indicate a significant (30–130 degrees) rotation between the magnetic cloud and pre-eruption filament axes [*Marubashi*, 1997; *Webb et al.*, 2000; *Rust and Labonte*, 2005]. It has been suggested that this rotation is due to kink-instability induced writhing during eruption [*Rust et al.*, 2005]. *Démoulin* [2008] reanalyzed the events described by *Marubashi* [1997], and found, for four of the five cases where the magnetic cloud axis was rotated greater than 30 degrees relative to the filament axis, that the direction-of-rotation/sign-of-helicity relationship found for erupting filaments by *Green et al.* [2007] held true, as would be expected if this axis rotation was caused by the kink instability.

[29] If our original, pre-eruption flux rope was oriented with its positive field originating south of its neutral line (as might be appropriate for an even-numbered solar cycle), and if it had erupted without writhing or reconnection, the interplanetary magnetic cloud resulting from it would have been classified as NWS in the notation of [*Bothmer and Schwenn*, 1997]. That is, the magnetic field vector at the center of the magnetic cloud would be directed northward in its leading portion, turn westward near cloud center, and be oriented southward in its trailing portion. Figures 11a–11c demonstrate this for an equilibrium flux rope [*Fan and Gibson*, 2006] (this equilibrium rope is actually rotated slightly counterclockwise from the original model rope's NWS orientation because it has writhed somewhat in finding an equilibrium; see *Fan and Gibson* [2006] for discussion). We have also plotted the more standard line-plot representation of the vector field along a trajectory through the cloud (Figure 12): the equilibrium rope is represented by the blue profiles, and the intersection of this trajectory on the slices of Figures 11a–11c as blue dots. (Note the trajectory is slightly away from the center of the slice: owing to the model symmetries, the radial component of the field would be exactly zero there.) For the partially ejected rope discussed in this paper, the leading portion of the rope has rotated by approximately 115 degrees, so that the portion of a magnetic cloud associated with that leading portion would be close to ENW, and, with an axis so highly inclined relative to the ecliptic, it would be categorized as "unipolar" [*Mulligan et al.*, 1998] (Figures 11d–11f), and green profiles in Figure 12).

[30] Such an axial rotation may significantly impact the geoeffectiveness of a magnetic cloud. Magnetic clouds possessing a strong southward magnetic field component (B_z) are more geoeffective [*Gonzalez and Tsurutani*, 1987]. Whether a southward component is more geoeffective at the front of the magnetic cloud or at its back is an issue of debate, but recent statistical studies indicate that they are more or less equivalent [*Li and Luhmann*, 2004; *Huttunen et al.*, 2005]. On the other hand, if a magnetic cloud is unipolar with a central axis pointing southward, it is particularly geoeffective, whereas if it is unipolar pointing northward, it is not [*Huttunen et al.*, 2005] (note that this study decoupled the geoeffectiveness of the magnetic cloud from that of the "sheath" region in front of it, which is often itself highly geoeffective).

[31] The rotation of our flux rope during eruption thus apparently took it from a configuration likely to be geoeffective (NWS) to one unlikely to be geoeffective (ENW, and more precisely, SE-NW). Or did it? The rotation was not the only change during eruption; as we have described in detail above, there were also reconnections, both internal to the erupting rope and with surrounding fields. Figures 11d–11g and 12 (green profiles) demonstrate that the magnetic vector in the cloud continues to rotate, so that its classification should actually be ENWS since it ultimately rotates >270 degrees. We now show how these combined changes in helicity, connectivity, and orientation have led to a change in topology for our escaping rope.

5.3. Changes in Topology

5.3.1. Magnetic Cloud Topologies

[32] The classic model for a magnetic cloud is that of a cylindrically symmetric, constant-α force-free flux rope [e.g., *Lundquist*, 1950]. Recent work, however, has demonstrated that departures from this form, such as ropes with distended cross sections, provide better fits to multipoint observations of magnetic clouds [*Mulligan and Russell*, 2001]. Another departure from the standard cylindrical flux rope is a rope in the form of a detached torus or spheromak [*Vandas et al.*, 1993], invoked to explain observations of magnetic clouds in which the component of the magnetic field along the projected solar North Pole, B_z, undergoes a double zero crossing implying a field vector rotating >270° [see, e.g., *Marubashi and Lepping*, 2007]. *Vandas et al.* [1998] demonstrated that viewing an "equatorial" passage of a detached speromak (i.e., a speromak possessing a core axis oriented perpendicular to the radial direction) would result in such magnetic cloud profiles. However, they found via a numerical simulation that interaction with the ambient solar wind would tend to rotate such a structure so that its

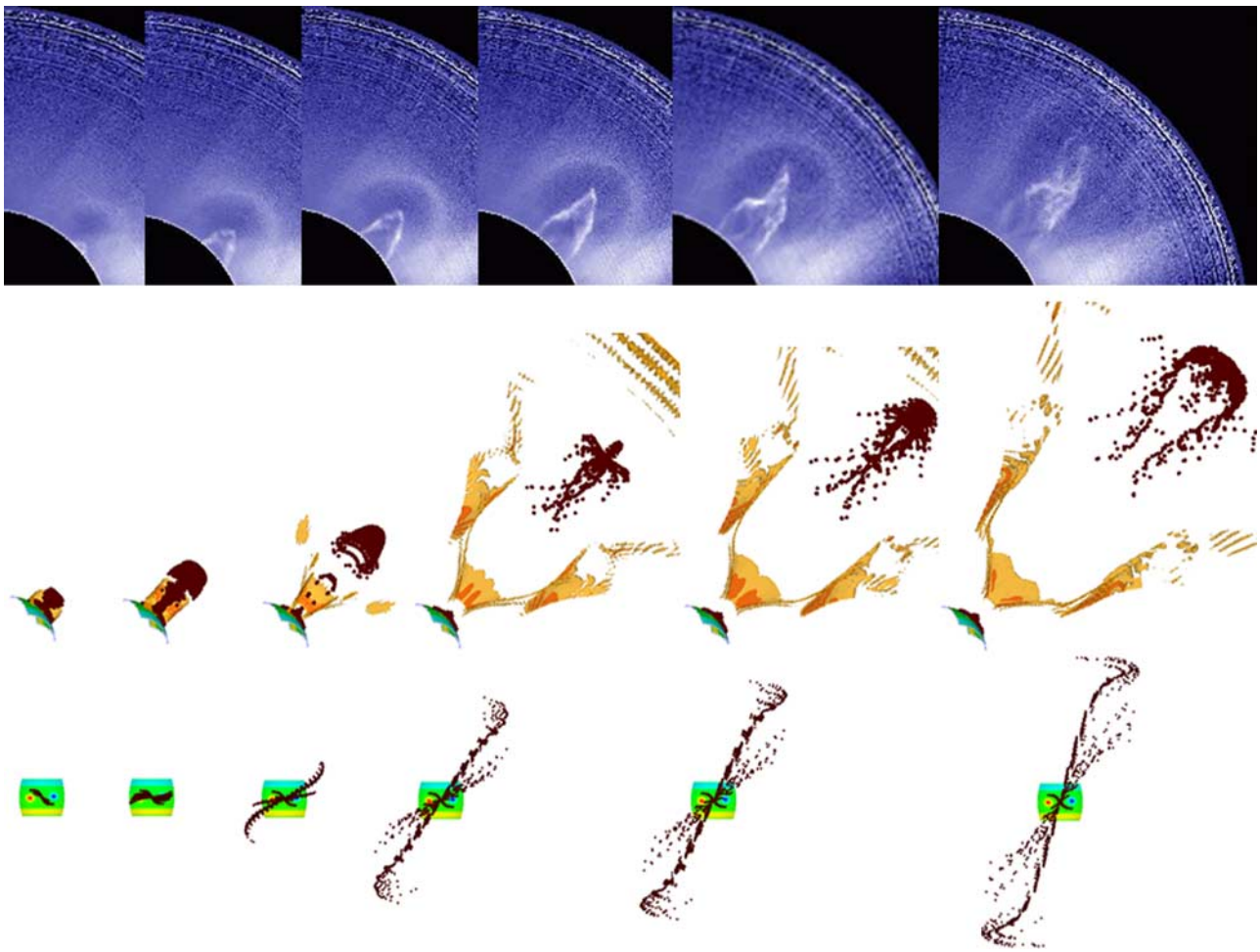

Figure 10. (top row) The 18 February 2003 CME observed by the Mauna Loa Solar Observatory Mk4 white light coronagraph. The core of the CME exhibits counterclockwise rotation. (middle and bottom rows) Simulated filament eruption as presented by *Gibson and Fan* [2006b], as viewed from the side and from above, also exhibiting counterclockwise rotation. The dark brown dots track evolving, initially dipped field and represent the partially erupting filament, with current sheets shown as red/light brown isosurfaces (middle row only). Left to right: time steps 86, 92, 106, 110, and 114. (See dynamic content Animation 6 in the HTML for a movie showing animations of the top and middle rows.)

axis was oriented radially by the time it arrived at the Earth and it would no longer result in a double zero-crossing of B_z (in fact, the B_z profile would essentially appear like that of a cylindrically symmetric rope). Moreover, a detached spheromak or torus is inconsistent with observations of counterstreaming suprathermal electrons commonly associated with magnetic clouds, which are generally interpreted as evidence of a magnetic structure still attached to the Sun at both ends [*Gosling et al.*, 1987].

[33] An alternative would be a "tethered spheromak" of the form presented by *Gibson and Low* [1998]. In this fully three-dimensional, analytic model, one end of a spheromak is contracted into the origin yielding a closed spheroidal (e.g., tear-shaped) flux system embedded in an otherwise open magnetic field. The self-similar expansion of this structure forms the basis of the model for a CME. Figures 13c and 13d show sample field lines of the tethered spheromak, demonstrating that while some field lines ergodically fill flux surfaces of detached tori (e.g., the red field line), these are embedded in field lines which remain attached to the solar surface (e.g., the purple and black field lines). This dual topology arises because the contraction of the bottom of the spheromak into the origin means that field lines lying on the outer flux surfaces cannot detach, and so are effectively line-tied as they expand outward.

5.3.2. Observational Implications of a Tethered Spheromak

[34] Figures 11h–11k and Figure 12 (red profiles) demonstrate that the field vector rotates over 270° at the center of the Gibson-Low tethered spheromak, so that it could indeed explain magnetic clouds with double B_z zero-crossing [e.g., *Vandas et al.*, 1993; *Dasso et al.*, 2007]. The amount of rotation of the field vector would of course be sensitive to which part of the magnetic structure passes by the observer (thus the magnetic cloud's trajectory). Also, it is important to point out that the degree of contraction of the spheromak to the origin (a model parameter) affects the amount of field rotation, and indeed the overall magnetic topology. A

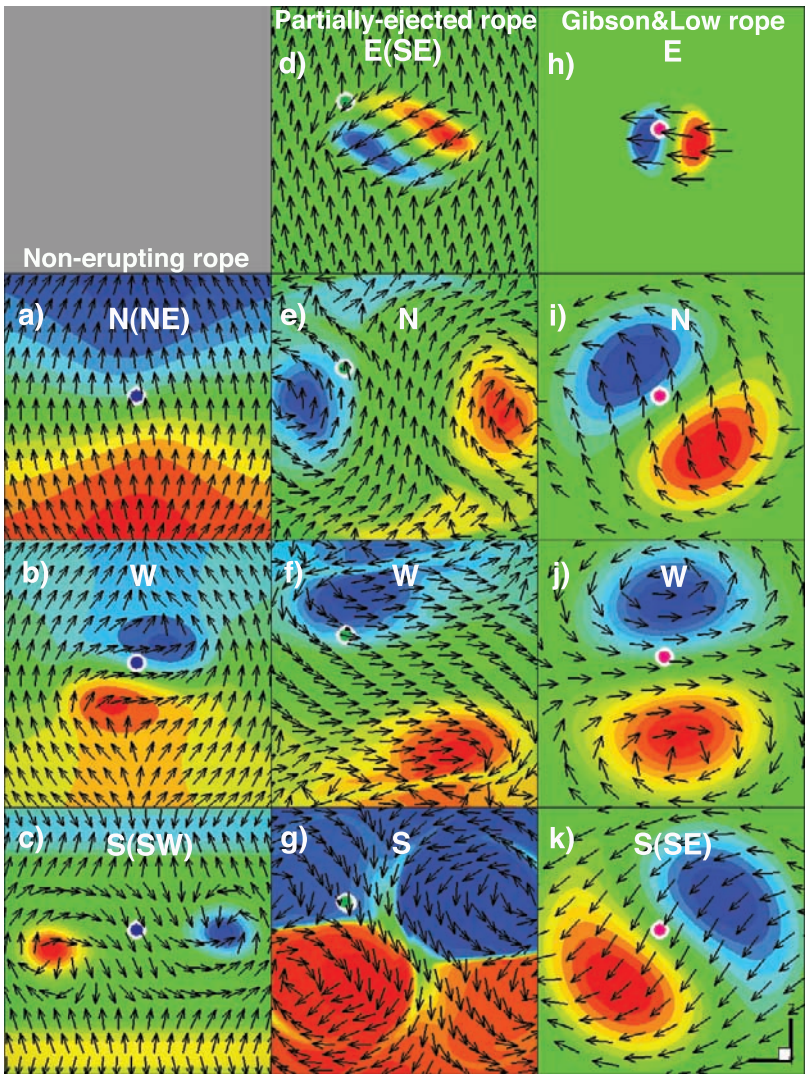

Figure 11. Model predictions of magnetic fields within magnetic clouds. Slices showing magnetic field at (a) top, (b) middle, and (c) lower boundary of an equilibrium flux rope [*Fan and Gibson*, 2006] equivalent to the pre-eruption rope of *Gibson and Fan* [2006b]. Slices showing magnetic field near (d) top, (e and f) middle, and (g) bottom of escaping portion of our partially ejected flux rope (time step 130). Slices showing magnetic field near (h) top, (i and j) middle, and (k) bottom of a *Gibson and Low* [1998] tethered spheromak. The blue dots in the left column, green dots in the middle column, and red dots in the right column correspond to the position where the magnetic field vector is measured versus decreasing height, or equivalently increasing time for a structure flying past the Earth, as shown in Figure 12. The colored isocontours indicate radial magnetic field through the slice (red positive, blue negative): note the color table is rescaled to the maximum/minimum radial field for each height. The vectors show the direction of the planar component of the magnetic field for each slice, and this direction is also indicated by the large white letters (solar north/south/east/west, where north is in the $+z$ direction of our simulation and west is in the $-x$ direction). A movie of the variation of magnetic field components in slices moving from top to bottom for the partially ejected rope versfsus the tethered spheromak is provided as dynamic content Animation 7 in the HTML. Note that the vectors in Animation 7 are scaled relative to the maximum radial field of each slice.

spheromak is characterized by both toroidal and poloidal winding, so that it possesses two axes of rotation, as indicated in Figures 13c and 13d by the red and black field lines. If all of the field at and below the bottom of the toroidal axis (located at the center of red torus) is contracted to the origin, there will be no detached field at all. In this case, the topology would be that of a deformed cylindrical flux rope, rather than a dual-topology rope possessing both toroidal and deformed cylindrical flux rope lines as shown in Figures 13c and 13d.

[35] The dual-topology rope, or tethered spheromak, can explain over-rotation within a magnetic cloud, and, because it is tethered, avoids the observational shortfalls of a completely detached spheromak. The realignment of a

detached spheromak during transit through the solar wind as found by *Vandas et al.* [1998] arises from draping of ambient magnetic field lines around the oblate toroidal body of the spheromak. It is likely that the tethered field lines surrounding any detached tori in the dual-topology case would suppress such an interaction, but it would be interesting to test this in a similar manner to *Vandas et al.* [1998] via a numerical heliospheric model. *Manchester et al.* [2004b] propagated a Gibson-Low type flux rope through the heliosphere in such a manner, and no such axial rotation was noted. However, the parameters chosen for the initial flux rope setup in that simulation were such that there were no detached toroidal field lines above the photosphere (where line-tying was enforced), so that the magnetic structure being propagated was actually a deformed cylindrical flux rope rather than a tethered spheromak. A test of how a tethered spheromak might evolve as it transits through the solar wind remains as an interesting subject for future study.

[36] A second observational shortfall of a fully detached spheromak magnetic cloud model is that it would predict a complete dropout in the flux of suprathermal electrons within the magnetic cloud. For the tethered spheromak, however, counter-streaming (bidirectional) suprathermal electrons could still be present within the magnetic cloud because much of its volume would be filled with field lines still attached to the lower boundary. Some degree of dropout in electron heat flux would still be expected owing to the nested detached field lines, and indeed such sporadic heat flux dropouts are sometimes observed within magnetic clouds [*Gosling*, 1990; *Larson et al.*, 1997; *Malandraki et al.*, 2003; *Crooker et al.*, 2004; *Harra et al.*, 2007]. Heat-flux dropouts do not necessarily imply complete disconnection, since higher-energy electrons have been shown in some cases to persist despite the lack of heat flux electrons [*Lin and Kahler*, 1992]. Thus even field lines which wind many times (and so are very long) but still are connected to the Sun could give rise to a dropout. More generally, if a long and winding, but still-Sun-connected field line were intersected near one end, so that the distance to the Sun along it was relatively short in one direction, but very long in another, it could give rise to a unidirectional suprathermal electron signature. It is probable that further reconnections with surrounding open magnetic fields during the rope's transit through the wind would also generate unidirectional

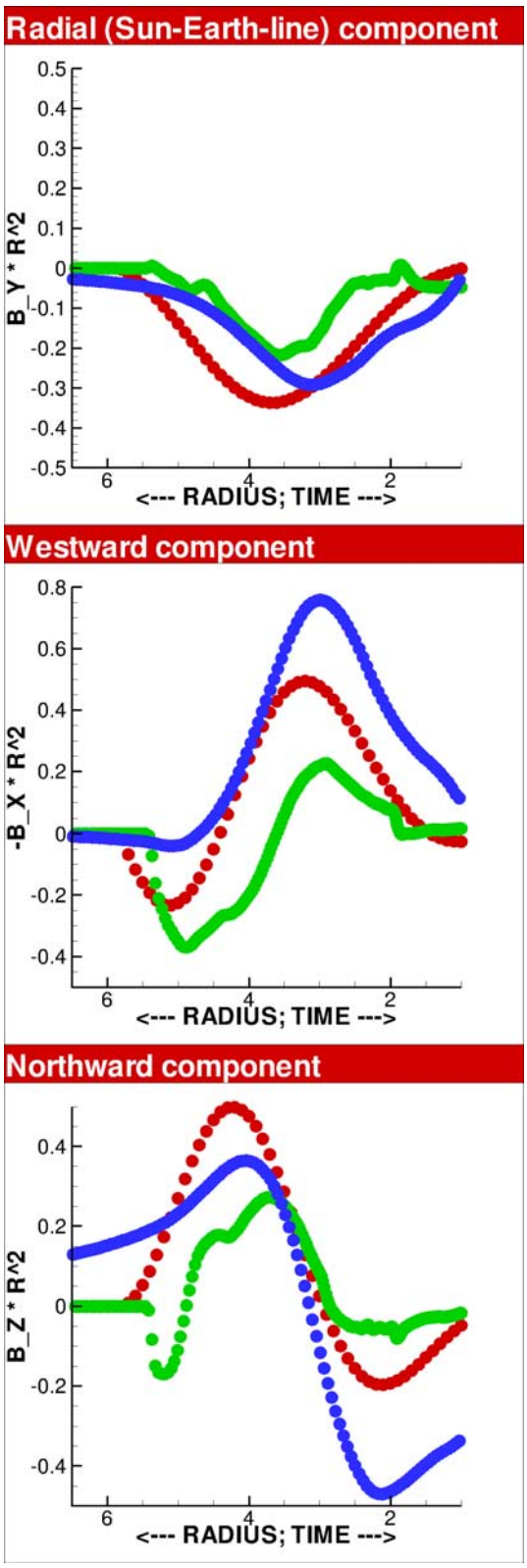

Figure 12. Model predictions of magnetic fields within magnetic clouds as in Figure 11, with plots showing the variation of the three components of magnetic field with height near the model central (y) axis (e.g., corresponding to the Sun-Earth line for an Earthward directed magnetic cloud). The locations of these trajectories are indicated on the planar slices of Figure 11 as colored dots. We plot magnetic field scaled by r^2 (in units of solar radii). Thus, assuming a radial expansion, the time variation of the components of magnetic field at the Earth as a magnetic cloud expands past it is effectively equivalent to moving downward through the modeled magnetic structures. Because these structures differ in size (and because we are interested in a side-by-side topological comparison), we have scaled the equilibrium rope of *Fan and Gibson* [2006] (left column of Figure 11) by a factor of $5r - 4$ (blue profiles) and the escaping portion of our partially ejected flux rope (middle column, Figure 11) by $r/3.5$ (green profiles), all relative to the model r of the *Gibson and Low* [1998] tethered spheromak model (right column, Figure 11) (red profiles).

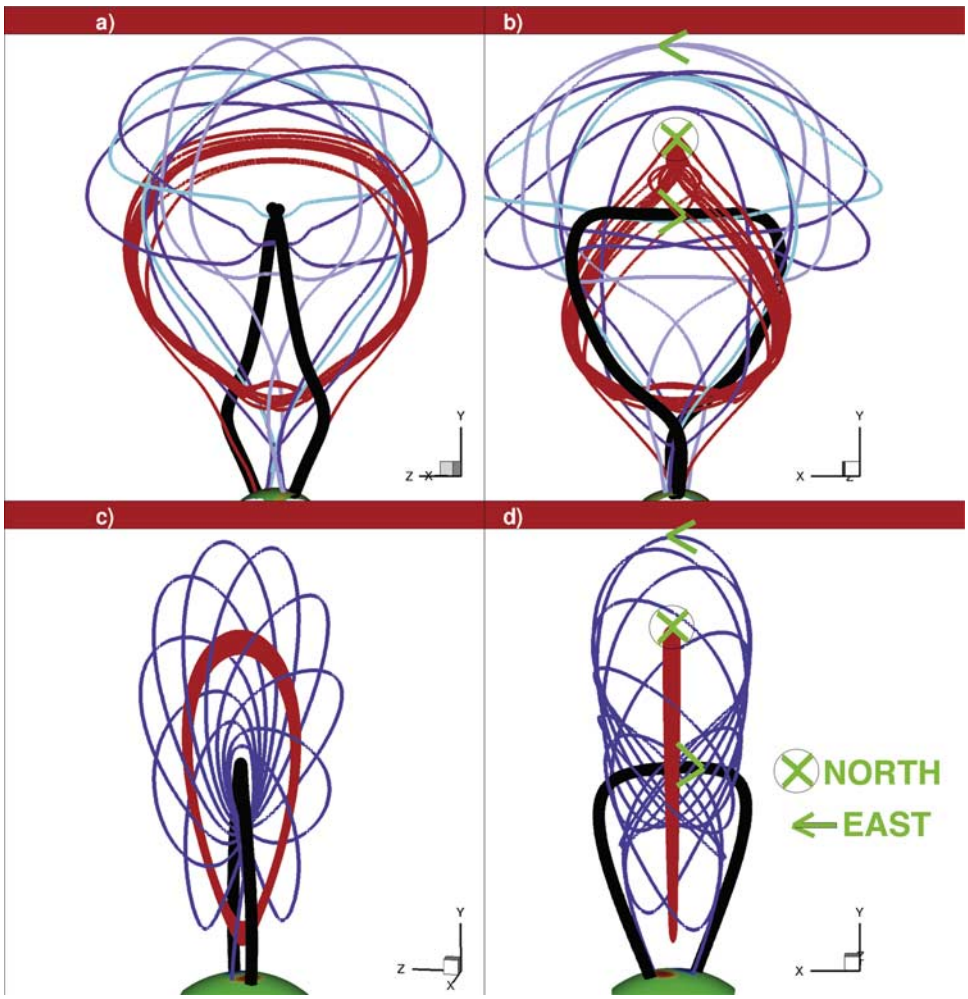

Figure 13. Sample field lines of partially ejected flux rope of (a and b) *Gibson and Fan* [2006a] (time step 106) and (c and d) *Gibson and Low* [1998] tethered spheromak. The thick black field lines in Figures 13a–13d represent the poloidal axes of the partially ejected rope and tethered spheromak, respectively. The red torus shown in Figures 13c and 13d is formed by a single field line ergodically covering a magnetic flux surface which encloses the spheromak toroidal axis. The partially ejected rope possesses a similarly toroidally winding single red field line, although it is not completely detached from the lower boundary. (See dynamic content Animation 8 in the HTML for a movie showing rotation of these model structures in three dimensions.)

streaming [*Gosling et al.*, 1995; *Crooker and Webb*, 2006], but it is interesting that even without such interchange reconnections, the tethered spheromak model is topologically complex enough to be consistent with observations of sporadic heat flux dropouts within otherwise bidirectional or unidirectional streaming electrons.

5.3.3. Formation of a Tethered Spheromak

[37] The question remains as to how such a tethered spheromak might be formed. One possibility suggested by *Lites and Low* [1997] is that it emerges from the solar interior already in a closed toroidal form. In that study and *Gibson and Low* [2000], a spheromak-type field configuration was shown to be consistent with pre-eruption prominence observations. Another possibility is that it could be formed during eruption [see, e.g., *Bellan and Hansen*, 1998]. A variety of models and simulations have demonstrated how reconnections during eruption, both internal and with external fields, could lead in general to mixed topologies within magnetic clouds [e.g., *Gosling et al.*, 1995; *Birn et al.*, 2000; *Crooker and Horbury*, 2005; *Dasso et al.*, 2007]. We will now demonstrate that, via a combination of such reconnections and writhing motions, the originally simple cylindrical flux rope which erupts in our simulation [*Gibson and Fan*, 2006a] is transformed into a tethered spheromak that is topologically equivalent to that of *Gibson and Low* [1998].

[38] Figures 13a and 13b show sample field lines for the partially ejected rope at a somewhat earlier time step (time = 106) than shown in Figures 11 and 12 (time = 130). It shows a spheromak topology in the process of being formed. As described above, the tethered spheromak possesses two axes of rotation, illustrated by the black (poloidal) and red (toroidal) field lines in Figures 13c and 13d. The purple field line in Figure 13c winds about the black poloidal axis, demonstrating that the magnetic field curvature is locally convex at this axis (thus, just above the black axial line, the

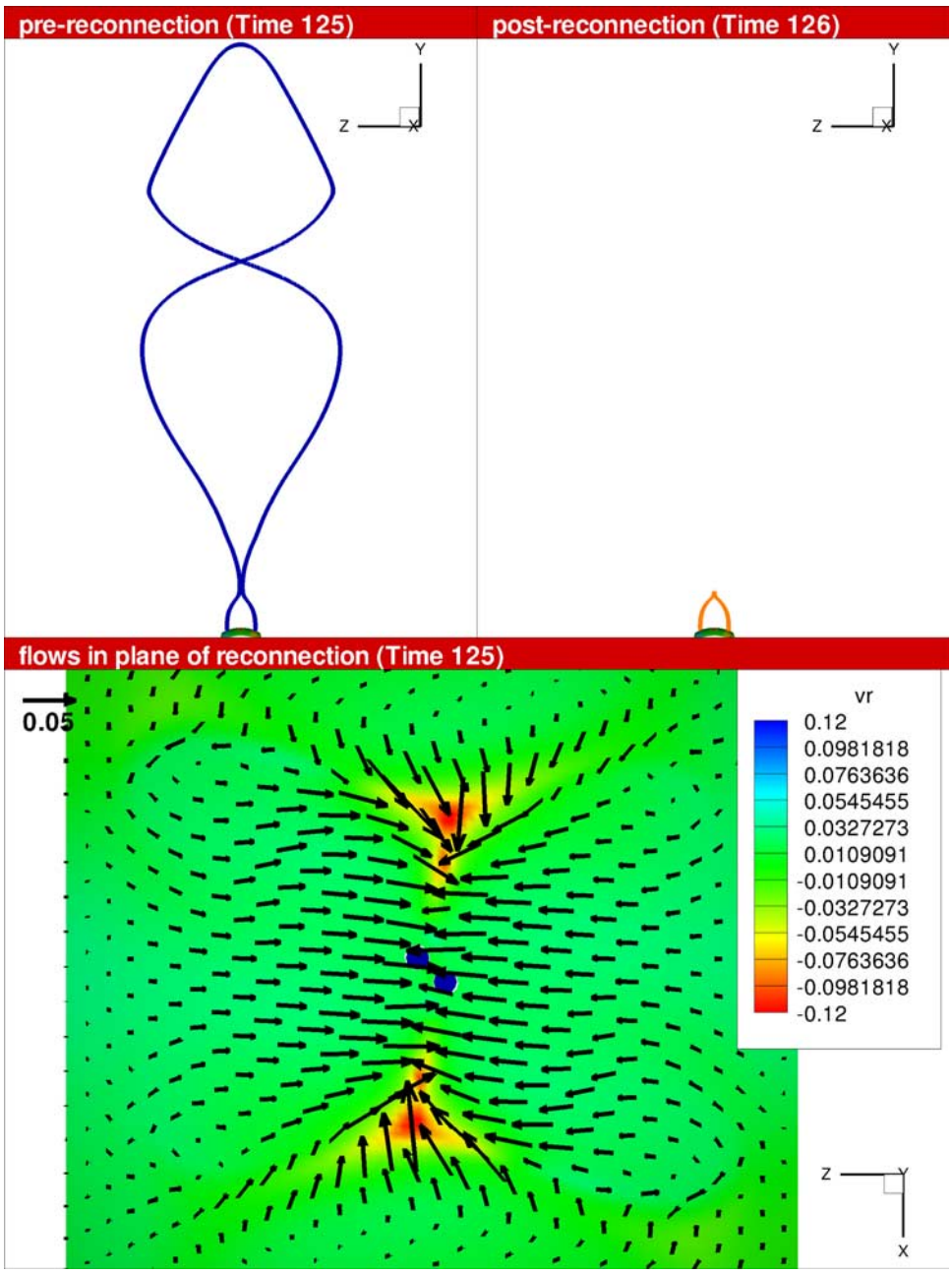

Figure 14. Special case of total flux detachment during flux-close-down reconnection. As in Figure 2, top images show pre-reconnection and post-reconnection field lines, and bottom image illustrates the convergence of the pre-reconnection field lines. Owing to the symmetries of the model, a field line can be found which reconnects with itself.

curvature of the field is downward, and just below, it is upward). By examining the local curvature of the field along the central *y* axis, we can identify an equivalent poloidal axis for the partially ejected rope, shown in Figures 13a and 13b by the thick black line, about which the blue and purple lines wind. We can also demonstrate that the partially ejected rope contains increasingly detached toroidal flux, as evidenced by the single red field line that winds about itself multiple times.

[39] The orientation at the top of this red, toroidally winding field line is predominantly northward, along the *z* axis (Figure 13b). Indeed, this top portion of the red field line corresponds to the central axis of the pre-eruption rope, which has rotated approximately 90 degrees by time 106: this may be seen by comparing to the brown dots of Figure 10 (bottom row), which track the initially dipped field lying just below the axis. The top of the rope has likewise rotated, pointing primarily eastward, along the model *x* axis. Thus, if one looks only at the top portion of the partially ejected rope, it appears similar to a cylindrical rope oriented just south of ENW (see, e.g., directions indicated in green on Figure 13b). If the eruption included a roughly 90 degree

writhe but no reconnections, this would indeed be the topology of the escaping rope.

[40] However, connectivity-mixing and flux-detaching reconnections create twist essentially in the manner described by in situ flux rope formation models [e.g., *Moore and Labonte*, 1980; *Gosling*, 1990; *Qiu et al.*, 2007], and the axial direction of this twist is that of the pre-eruption rope, i.e., westward (Figure 11b). Figure 4 illustrates this: although the top of the dark blue pre-reconnection field line has clearly writhed, the ''legs'' of this field line have not, so that the reconnection with the light blue arcade field line creates twist about the x axis (east-west). This is the origins of the poloidal axis of rotation which we have identified as the thick black line in Figures 13a and 13b (note that it has writhed approximately 30 degrees counterclockwise from east-west by time step 106).

[41] A side-by-side comparison of the tethered spheromak and partially ejected rope in Figures 11, 12 (red versus green), and 13 emphasizes the similarity in their topologies. One difference that remains between them is that the red, toroidally winding field line shown in Figures 13a and 13b is not a completely detached torus as in Figures 13c and 13d. However, it clearly has a large winding number, and, as close-down reconnections continue to occur, this winding will increase to the point that it may approach the ergodically winding limit of the analytic tethered spheromak. In fact, there is evidence that some portion of the simulation field does become completely disconnected. Figure 14 shows a reconnection occurring at time step 125, where a magnetic field line (blue, top left) meets itself at a current sheet, and detaches to leave a single, post-reconnection cusped field line (orange, top right). (There should be a corresponding, detached toroidal field line in the post-reconnection image, but finding this field line would be like finding the proverbial needle in hay stack because, unlike the cusped orange field line, it is not line-tied to the lower boundary.) We emphasize that such a self-reconnection is cosmically unlikely on the Sun, and only arises in our simulation because of its prescribed symmetries. Far more likely on the Sun (and even in our simulation) are the reconnections between neighboring field lines as shown in Figure 7, which, although they may not create toroidal field lines that ''meet their own tail'', create field lines that wind so much and are long enough so as to be effectively disconnected from the solar surface.

6. Conclusions

[42] The three-dimensionality of coronal magnetic fields is a fundamental aspect of CMEs, and the partial-ejection of magnetic flux ropes manifested in our simulations is characteristic of the resulting complexity of eruptions. In this paper we demonstrate that such complexity directly affects how interplanetary CMEs are linked to their sources at the Sun. We now summarize our findings, and describe their broader implications for understanding and ultimately predicting space weather.

[43] First of all, because a significant fraction of magnetic helicity remains behind after a partial ejection, the source region may be prone to multiple eruptions as further helicity is injected, either through magnetic flux emergence or photospheric shearing motion. This is important for space weather prediction and interpretation, since multiple CMEs from the same region have been shown to lead to particularly strong solar energetic particle (SEP) events [*Gopalswamy et al.*, 2004]. SEP events are a primary source of concern for current spacecraft operation and future extended manned space missions [*Klecker*, 1996].

[44] Moreover, because the escaping portion of the rope writhes and reconnects, both internally and with surrounding fields, a tethered spheromak topology is formed during the rope's partial ejection. This is an important possibility to consider because most analyses of magnetic clouds assume a cylindrical magnetic rope topology in fitting to observations, yet some observations do not fit this standard model [*Vandas et al.*, 1998; *Dasso et al.*, 2007]. Such a topological change would affect the accuracy of a wide range of interpretive techniques currently used to connect magnetic clouds to their source, regarding magnetic flux, helicity, and axial orientation (*Démoulin* [2008] and references therein). Predicting these properties, in particular as they relate to southward-pointing magnetic field, is important for an accurate assessment of whether a magnetic cloud is likely to be geoeffective.

[45] It is important to emphasize that the tethered-spheromak topology differs from previous magnetic cloud models invoking spheromaks in that large portions of the field remains tethered at the sun. Indeed, we have described how detached, doubly attached, and apparently open fields could intermingle within this structure. We have also described how the initial location of transient coronal holes during an eruption may be misleading as clues to how magnetic clouds relate to their sources at the Sun, if they appear beneath stretched out magnetic field which subsequently changes connectivity [*Mandrini et al.*, 2007]. Our simulation illustrates this, and moreover predicts a two-stage movement of transient coronal hole boundaries away from a central core active region consistent with observations [*Reinard and Biesecker*, 2008]. Understanding the connectivity between magnetic cloud and transient coronal hole is important for prediction, for example, of high-speed streams following ICMEs which have the potential to increase geoeffectiveness [*McIntosh et al.*, 2007].

[46] In conclusion, our analysis suggests that close attention should be paid to coronal observations during eruption to determine the degree of writhing motions and/or reconnections with surrounding fields. We note that recent observations indicating reconnections in solar wind magnetic fields [*Gosling*, 2007] emphasize that the flux rope's journey does not end in the corona. If we wish to be able to predict and interpret magnetic structures passing the Earth, we need to build as complete a picture as possible about their origins and evolution as they traverse the heliosphere.

[47] **Acknowledgments.** We thank the referees for valuable input to the paper, and Mike Wiltberger for HAO internal review of this manuscript. We also thank Giuliana de Toma, Craig Deforest, Jack Gosling, Hugh Hudson, Yan Li, Dana Longcope, B. C. Low, Janet Luhmann, Scott McIntosh, Jiong Qiu, and Alysha Reinard for numerous helpful discussions. The Transition Region and Coronal Explorer, TRACE, is a mission of the Stanford-Lockheed Institute for Space Research (a joint program of the Lockheed-Martin Advanced Technology Center's Solar and Astrophysics Laboratory and Stanford's Solar Observatories Group), and part of the NASA Small Explorer program. SOHO is a project of international cooperation between ESA and NASA. The Soft X-Ray Telescope (SXT)

was prepared by the Lockheed Palo Alto Research Laboratory, the National Astronomical Observatory of Japan, and the University of Tokyo with the support of NASA and ISAS. The Mauna Loa Solar Observatory is a facility of the National Center for Atmospheric Research, which is sponsored by the National Science Foundation.

[48] Amitava Bhattacharjee thanks the reviewers for their assistance in evaluating this paper.

References

Alexander, D., R. Liu, and H. Gilbert (2006), Hard x-ray production in a failed filament eruption, *Astrophys. J.*, *653*, 719.

Attrill, G., M. S. Nakwacki, L. K. Harra, L. Van Driel-Gesztelyi, C. H. Mandrini, S. Dasson, and J. Wang (2006), Using the evolution of coronal dimming regions to probe the global magnetic field topology, *Sol. Phys.*, *238*, 117.

Attrill, G., L. K. Harra, L. K. Van Driel-Gesztelyi, and P. Demoulin (2007), Coronal "wave": Magnetic footprint of a coronal mass ejection?, *Astrophys. J. Lett.*, *656*, 101.

Bellan, P. M., and J. F. Hansen (1998), Laboratory simulations of solar prominence eruptions, *Phys. Plasmas*, *5*, 1991.

Berger, M. A., and G. B. Field (1984), The topological properties of magnetic helicity, *J. Fluid Mech.*, *147*, 133.

Birn, J. T., J. T. Gosling, M. Hesse, T. G. Forbes, and E. R. Priest (2000), Simulations of three-dimensional reconnection in the solar corona, *Astrophys. J.*, *541*, 1078.

Birn, J. T., T. G. Forbes, and M. Hesse (2006), Stability and dynamic evolution of three-dimensional flux ropes, *Astrophys. J.*, *645*, 732.

Bothmer, V., and R. Schwenn (1997), The structure and origin of magnetic clouds in the solar wind, *Ann. Geophys.*, *16*, 1.

Burlaga, L. F. (1988), Magnetic clouds and force-free fields with constant alpha, *J. Geophys. Res.*, *93*, 7217.

Burlaga, L. F., L. Klein, N. R. J. Sheeley, D. J. Michels, R. Howard, M. J. Koomen, R. Schwenn, and H. Rosenbauer (1982), A magnetic cloud and a coronal mass ejection, *Geophys. Res. Lett.*, *9*, 1317.

Cremades, H., and V. Bothmer (2004), On the three-dimensional configuration of coronal mass ejections, *Astron. Astrophys.*, *422*, 307.

Crooker, N., and T. S. Horbury (2005), Solar imprint on icmes, their magnetic connectivity, and heliospheric evolution, *Space Sci. Rev.*, *123*, 93.

Crooker, N. U., and D. F. Webb (2006), Remote sensing of the solar site of interchange reconnection associated with the May 1997 magnetic cloud, *J. Geophys. Res.*, *111*, A08108, doi:10.1029/2006JA011649.

Crooker, N. U., R. Forsyth, A. Rees, J. T. Gosling, and S. W. Kahler (2004), Counterstreaming electrons in magnetic clouds near 5 AU, *J. Geophys. Res.*, *109*, A06110, doi:10.1029/2004JA010426.

Dasso, S., M. S. Nakwacki, P. Demoulin, and C. H. Mandrini (2007), Progressive transformation of a flux rope to an ICME, *Sol. Phys.*, *244*, 115.

de Toma, G., T. E. Holzer, J. T. Burkepile, and H. R. Gilbert (2005), Transient coronal holes as seen in the He I 1083 nm MLSO observations, *Astrophys. J.*, *621*, 1109.

Delannee, C. (2000), Another view of the EIT wave phenomenon, *Astrophys. J.*, *545*, 512.

Delannee, C., J.-F. Hochedez, and G. Aulanier (2007), Stationary parts of an EIT and Moreton wave: A topological model, *Astron. Astrophys.*, *465*, 603.

Démoulin, P. (2008), Quantitative links between cmes and magnetic clouds, *Ann. Geophys.*, *25*, 1.

Dere, K. P., G. E. Brueckner, R. A. Howard, D. J. Michels, and J. P. Delaboudiniere (1998), LASCO and EIT observations of helical structure in coronal mass ejections, *Astrophys. J.*, *492*, 804.

Fan, Y. (2005), Coronal mass ejections as loss of confinement of kinked magnetic flux ropes, *Astrophys. J.*, *630*, 543.

Fan, Y., and S. E. Gibson (2003), The emergence of a twisted magnetic flux tube into a preexisting coronal arcade, *Astrophys. J. Lett.*, *589*, 505.

Fan, Y., and S. E. Gibson (2004), Numerical simulations of three-dimensional coronal magnetic fields resulting from the emergence of twisted magnetic flux tubes, *Astrophys. J.*, *609*, 1123.

Fan, Y., and S. E. Gibson (2006), On the nature of the x-ray bright core in a stable filament channel, *Astrophys. J. Lett.*, *641*, 149.

Fan, Y., and S. E. Gibson (2007), Onset of coronal mass ejections due to loss of confinement of coronal flux ropes, *Astrophys. J.*, *668*, 1232.

Gibson, S. E., and Y. Fan (2006a), The partial expulsion of a magnetic flux rope, *Astrophys. J. Lett.*, *637*, 65.

Gibson, S. E., and Y. Fan (2006b), Coronal prominence structure and dynamics: A magnetic flux rope interpretation, *J. Geophys. Res.*, *111*, A12103, doi:10.1029/2006JA011871.

Gibson, S. E., and Y. Fan (2006c), Partially-ejected flux ropes: Implications for space weather, in *Solar Activity and Its Magnetic Origin*, p. 319, Cambridge Univ. Press, Cambridge, U. K.

Gibson, S. E., and B. C. Low (1998), A time-dependent three-dimensional magnetohydrodynamic model of the coronal mass ejection, *Astrophys. J.*, *493*, 460.

Gibson, S. E., and B. C. Low (2000), Three-dimensional and twisted: An MHD interpretation of on-disk observational characteristics of coronal mass ejections, *J. Geophys. Res.*, *105*, 18,187.

Gibson, S. E., et al. (2002), The structure and evolution of a sigmoidal active region, *Astrophys. J.*, *574*, 265.

Gilbert, H. R., T. E. Holzer, J. T. Burkepile, and A. J. Hundhausen (2000), Active and eruptive prominences and their relationship to coronal mass ejections, *Astrophys. J.*, *537*, 503.

Gilbert, H. R., D. Alexander, and R. Liu (2007), Filament kinking and its implications for eruption and re-formation, *Sol. Phys.*, *245*, 287.

Gonzalez, W. D., and B. T. Tsurutani (1987), Criteria of interplanetary parameters causing intense magnetic storms (Dst < -100 nt), *Planet. Space Sci.*, *35*, 1101.

Gopalswamy, N., S. Yashiro, S. Krucker, G. Stenborg, and R. A. Howard (2004), Intensity variation of large solar energetic particle events associated with coronal mass ejections, *J. Geophys. Res.*, *109*, A12105, doi:10.1029/2004JA010602.

Gosling, J. T. (1990), Coronal mass ejections and magnetic flux ropes in interplanetary space, in *Physics of Magnetic Flux Ropes, Geophys. Monogr. Ser.*, vol. 58, edited by C. T. Russell, E. R. Priest, and L. C. Lee, p. 343, AGU, Washington, D. C.

Gosling, J. T. (1997), Coronal mass ejections: An overview, in *Coronal Mass Ejections, Geophys. Monogr. Ser.*, vol. 99, edited by N. Crooker, J. A. Joselyn, and J. Feynman, p. 9, AGU, Washington, D. C.

Gosling, J. T. (2007), Observations of magnetic reconnections in the turbulent high-speed solar wind, *Astrophys. J. Lett.*, *671*, 73.

Gosling, J. T., D. N. Baker, S. J. Bame, W. C. Feldman, R. D. Zwickl, and E. J. Smith (1987), Bidirectional solar wind electron heat flux events, *Sol. Phys.*, *92*, 8519.

Gosling, J. T., J. Birn, and M. Hesse (1995), Three-dimensional magnetic reconnection and the magnetic topology of coronal mass ejection events, *Geophys. Res. Lett.*, *22*(9), 869.

Green, L. M., B. Kliem, T. Toeroek, L. van Driel-Gesztelyi, and G. D. R. Attrill (2007), Transient coronal sigmoids and rotating erupting flux ropes, *Sol. Phys.*, *246*, 345.

Harra, L. K., et al. (2007), How does large flaring activity from the same active region produce oppositely directed magnetic clouds?, *Sol. Phys.*, *244*, 95.

Hirayama, T. (1974), Theoretical model of flares and prominences. I: Evaporating flare model, *Sol. Phys.*, *34*, 323.

Hudson, H. S., J. R. Lemen, O. C. St. Cyr, A. C. Sterling, and D. F. Webb (1998), X-ray coronal changes during halo CMES, *Geophys. Res. Lett.*, *25*, 2481.

Huttunen, K. E. J., R. Schwenn, V. Bothmer, and H. E. J. Koskinen (2005), Properties and geoeffectiveness of magnetic clouds in the rising, maximum and early declining phases of solar cycle 23, *Ann. Geophys.*, *23*, 625.

Ji, H., H. Wang, E. J. Schmahl, Y.-J. Moon, and Y. Jiang (2003), Observations of the failed eruption of a filament, *Astrophys. J.*, *595*, 135.

Kahler, S. W., and H. S. Hudson (2001), Origin and development of transient coronal holes, *J. Geophys. Res.*, *106*, 29,239.

Klecker, B. (1996), Energetic particle environment in near-Earth orbit, *Adv. Space Res.*, *17*(2), 237.

Klein, L. W., and L. F. Burlaga (1982), Interplanetary magnetic clouds at 1 AU, *J. Geophys. Res.*, *87*, 613.

Ko, Y.-K., et al. (2005), Multialtitude observations of a coronal jet during the third whole sun month campaign, *Astrophys. J.*, *623*, 519.

Larson, D. E., et al. (1997), Tracing the topology of the october 18–20, 1995, magnetic cloud with $\sim$0.1–102 keV electrons, *Geophys. Res. Lett.*, *24*(15), 1911.

Leamon, R. J., R. C. Canfield, S. L. Jones, K. Lambkin, B. J. Lundberg, and A. A. Pevtsov (2004), Helicity of magnetic clouds and their associated active regions, *J. Geophys. Res.*, *109*, A05106, doi:10.1029/2003JA010324.

Lepping, R. P., L. F. Burlaga, and J. A. Jones (1990), Magnetic field structure of interplanetary magnetic clouds at 1 AU, *J. Geophys. Res.*, *95*, 11,957.

Li, Y., and J. Luhmann (2004), Solar cycle control of the magnetic cloud polarity and the geoeffectiveness, *J. Atmos. Sol. Terr. Phys.*, *66*, 323.

Lin, J., and T. G. Forbes (2000), Effects of reconnection on the coronal mass ejection process, *J. Geophys. Res.*, *105*, 2375.

Lin, R. P., and S. W. Kahler (1992), Interplanetary magnetic field connection to the Sun during heat flux dropouts in the solar wind, *J. Geophys. Res.*, *97*, 8203.

Lites, B. W., and B. C. Low (1997), Flux emergence and prominences: A new scenario for 3-dimensional field geometry based on observations with the advanced Stokes polarimeter, *Sol. Phys.*, *174*, 91.

Liu, R., D. Alexander, and H. R. Gilbert (2007), Kink-induced catastrophe in a coronal eruption, *Astrophys. J.*, *661*, 1260.
Liu, R., D. Alexander, and H. R. Gilbert (2008), The effect of magnetic reconnection and writhing in a partial filament eruption, *Astrophys. J.*, *680*, 1508.
Lundquist, S. (1950), Magnetohydrostatic fields, *Ark. Fys.*, *2*, 361.
Mackay, D. H., and A. A. van Ballegooijen (2006), Models of the large-scale corona. I. Formation, evolution, and liftoff of magnetic flux ropes, *Astrophys. J.*, *641*, 577.
Malandraki, O. E., E. T. Sarris, and G. Tsiropoula (2003), Magnetic topology of coronal mass ejection events out of the ecliptic: Ulysses/HI-SCALE energetic particle observations, *Ann. Geophys.*, *21*, 1249.
Manchester, W., T. Gombosi, D. DeZeeuw, and Y. Fan (2004a), Eruption of a buoyantly emerging magnetic flux rope, *Astrophys. J.*, *610*, 588.
Manchester, W. B., IV, T. I. Gombosi, I. Roussev, A. Ridley, D. L. De Zeeuw, I. V. Sokolov, K. G. Powell, and G. Tóth (2004b), Modeling a space weather event from the Sun to the Earth: CME generation and interplanetary propagation, *J. Geophys. Res.*, *109*, A02107, doi:10.1029/2003JA010150.
Mandrini, C. H., S. Pohjolainen, S. Dasso, L. M. Green, P. Demoulin, L. van Driel-Gesztelyi, C. Copperwheat, and C. Foley (2005), Interplanetary flux rope ejected from an x-ray bright point, *Astron. Astrophys.*, *434*, 725.
Mandrini, C. H., M. S. Nakwacki, G. Attrill, L. van Driel-Gesztelyi, P. Demoulin, S. Dasso, and H. Elliott (2007), Are CME-related dimmings always a simple signature of interplanetary magnetic cloud footpoints?, *Sol. Phys.*, *244*, 25.
Marubashi, K. (1997), Interplanetary magnetic flux ropes and solar filaments, in *Coronal Mass Ejections, Geophys. Monogr. Ser.*, vol. 99, p. 147, AGU, Washington, D. C.
Marubashi, K., and R. P. Lepping (2007), Long-duration magnetic clouds: A comparison of analyses using torus- and cylinder-shaped flux rope models, *Ann. Geophys.*, *25*, 2453.
McIntosh, S. W., R. J. Leamon, A. R. Davey, and M. J. Wills-Davey (2007), The posteruptive evolution of a coronal dimming, *Astrophys. J.*, *660*, 1653.
Moore, R. L., and B. J. Labonte (1980), The filament eruption in the 3b flare of July 29, 1973: Onset and magnetic field configuration, in *Solar and Interplanetary Dynamics*, p. 207, Int. Astron. Union, Paris.
Mulligan, T., and C. T. Russell (2001), Multispacecraft modeling of the flux rope structure of interplanetary coronal mass ejections: Cylindrically symmetric versus nonsymmetric topologies, *J. Geophys. Res.*, *106*, 10,581.
Mulligan, T., C. T. Russell, and J. G. Luhmann (1998), Solar cycle evolution of the structure of magnetic clouds in the inner heliosphere, *J. Geophys. Res.*, *25*, 2959.
Plunkett, S. P., A. Vourlidas, S. Simberova, M. Karlicky, P. Kotric, P. Heinzel, Y. A. Kupryakov, W. P. Guo, and S. T. Wu (2000), Simultaneous SOHO and ground-based observations of a large eruptive prominence and coronal mass ejection, *Sol. Phys.*, *194*, 371.
Qiu, J., and V. B. Yurchyshyn (2005), Magnetic reconnection flux and coronal mass ejection velocity, *Astrophys. J. Lett.*, *634*, 121.
Qiu, J., Q. Hu, T. A. Howard, and V. B. Yurchyshyn (2007), On the magnetic flux budget in low-corona magnetic reconnection and interplanetary coronal mass ejections, *Astrophys. J.*, *659*, 758.
Reinard, A. A., and D. A. Biesecker (2008), CME-associated coronal dimmings, *Astrophys. J.*, *674*, 576.
Roussev, I. L., N. Lugaz, and I. V. Sokolov (2007), New physical insight on the changes in magnetic topology during coronal mass ejections: Case studies for the 2002 April 21 and August 24 events, *Astrophys. J. Lett.*, *668*, 87.
Rust, D. M. (2003), Helical flux rope structure of solar filaments, *Adv. Space. Res.*, *32*(10), 1895.
Rust, D. M., and B. Labonte (2005), Observational evidence of the kink instability in solar filament eruptions and sigmoids, *Astrophys. J.*, *622*, 69.
Rust, D. M., B. J. Anderson, M. D. Andrews, M. H. Acuña, C. T. Russell, P. W. Schuck, and T. Mulligan (2005), Comparison of interplanetary disturbances at the near spacecraft with coronal mass ejections at the Sun, *Astrophys. J.*, *621*, 524.
Sterling, A. C., and H. S. Hudson (1997), Yohkoh SXTsxt observations of x-ray dimming associated with a halo coronal mass ejection, *Astrophys. J.*, *491*, 55.
Thompson, B. J., S. P. Plunkett, J. B. Gurman, J. S. Newmark, O. C. St. Cyr, and D. J. Michels (1998), SOHO/EIT observations of an Earth-directed coronal mass ejection on May 12, 1997, *Geophys. Res. Lett.*, *25*, 2465.
Thompson, B. J., E. W. Cliver, N. Nitta, C. Delannée, and J. P. Delaboudinière (2000), Correction to "Coronal dimmings and energetic CMEs in April–May 1998", *Geophys. Res. Lett.*, *27*, 1865.
Toeroek, T., and B. Kliem (2005), Confined and ejective eruptions of kink-unstable flux ropes, *Astrophys. J. Lett.*, *630*, 97.
Tokman, M., and P. M. Bellan (2002), Three-dimensional model of the structure and evolution of coronal mass ejections, *Astrophys. J.*, *567*, 1202.
Vandas, M. S., S. Fischer, P. Pelant, and A. Geranois (1993), Evidence for a spheroidal structure of magnetic clouds, *J. Geophys. Res.*, *98*, 21,061.
Vandas, M. S., S. Fischer, M. Dryer, Z. Smith, and T. Detman (1998), Propagation of a spheromak: 2. Three-dimensional structure of a spheromak, *J. Geophys. Res.*, *103*, 23,717.
Webb, D. F., R. P. Lepping, L. F. Burlaga, C. E. deForest, D. E. Larson, S. F. Martin, S. P. Plunkett, and D. M. Rust (2000), The origin and development of the May 1997 magnetic cloud, *J. Geophys. Res.*, *105*, 27,251.
Williams, D. R., T. Toeroek, P. Demoulin, L. van Driel-Gesztelyi, and B. Kliem (2005), Eruption of a kink-unstable filament in NOAA active region 10696, *Astrophys. J. Lett.*, *628*, 163.
Yurchyshyn, V. B., H. Wang, and P. R. Goode (2001), Orientation of the magnetic fields in interplanetary flux ropes and solar filaments, *Astrophys. J.*, *563*, 381.
Yurchyshyn, V. B., C. Liu, V. Abramenko, and J. Krall (2006), The May 13, 2005 eruption: Observations, data analysis and interpretation, *Sol. Phys.*, *239*, 317.
Zhang, Y., J. Wang, G. D. R. Attrill, L. K. Harra, Z. Yang, and X. He (2007), Coronal magnetic connectivity and EUV dimmings, *Sol. Phys.*, *241*, 329.
Zhou, G. P., J. X. Wang, J. Zhang, P. F. Chen, H. S. Ji, and K. Dere (2006), Two successive coronal mass ejections driven by the kink and drainage instabilities of an eruptive prominence, *Astrophys. J.*, *651*, 1238.
Zhukov, A. N., and I. S. Veselovsky (2007), Global coronal mass ejections, *Astrophys. J. Lett.*, *664*, 131.

Y. Fan and S. E. Gibson, High Altitude Observatory, National Center for Atmospheric Research, P.O. Box 3000, Boulder, CO 80307-3000, USA. (sgibson@hao.ucar.edu)